ILLINOIS

UNIVERSITY OF ILLINOIS AT URBANA-CHAMPAIGN

-

# PRODUCTION NOTE

University of Illinois at
Urbana-Champaign Library
Large-scale Digitization Project, 2007.

UNIVERSITY OF ILLINOIS ENGINEERING EXPERIMENT STATION BULLETIN NO. 426

# Inelastic Behavior of Ductile Members Under Dead Loading

by

M. E. Clark

H. T. Corten

O. M. Sidebottom

UNIVERSITY OF ILLINOIS BULLETIN

*Price: One Dollar*

UNIVERSITY OF ILLINOIS BULLETIN

Volume 52, Number 16; October, 1954. Published seven times each month by the University of Illinois. Entered as second-class matter December 11, 1912, at the post office at Urbana, Illinois, under the Act of August 24, 1912. Office of Publication, 207 Administration Building, Urbana, Ill.

# Inelastic Behavior of Ductile Members Under Dead Loading

by

M. E. Clark

ASSISTANT PROFESSOR OF
THEORETICAL AND APPLIED MECHANICS

H. T. Corten

ASSISTANT PROFESSOR OF
THEORETICAL AND APPLIED MECHANICS

O. M. Sidebottom

ASSOCIATE PROFESSOR OF
THEORETICAL AND APPLIED MECHANICS

ENGINEERING EXPERIMENT STATION BULLETIN NO. 426

3050—10-54—54901

UNIVERSITY
OF ILLINOIS
PRESS

## CONTENTS

## FIGURES

## FIGURES (Continued)



## TABLES

This page is intentionally blank.

# I. INTRODUCTION

## 1. Preliminary Statement

Since the turn of the century, considerable work of both theoretical and experimental nature has been undertaken to determine the inelastic behavior of load-carrying members in which the stress distribution is non-uniform. This interest has arisen due to the fact that the maximum utilizable load on the member may be appreciably increased by allowing only a small amount of inelastic deformation to occur in the member. A large portion of this work has been confined to the inelastic bending of beams. The early experimental work was performed on mild steel beams because of the prevalence of applications and the ease of theoretical treatment; however, the results obtained by several of these investigators[1, 2, 3, 4, 5]* led to the conclusion that the yield point of the mild steel itself was raised in the presence of a non-uniform distribution of stress. Three of the investigators, G. Cook,[1] F. Nakanishi,[2] and J. L. M. Morrison,[4] were speaking of the upper yield point in drawing their conclusions; however, they found that the lower yield point in the beam tests agreed closely with that found from standard tension tests. Other investigators[6, 7, 8, 9] indicate that in beams in which the upper yield point is eliminated, the lower yield point is not raised; rather, the increase in load-carrying capacity is altogether due to beneficial redistribution of stress accompanying the yielding in the member.

Similar conclusions were substantiated by several more investigators[7, 10, 11] who worked with materials like aluminum, magnesium, and annealed high carbon steel which exhibited strain-hardening characteristics throughout the inelastic range. In these recent investigations, the experimentally determined moment-deformation relations were found to agree closely with those obtained by a theoretical analysis based on the stress-strain relation as found from the simple tension test.

## 2. Purpose

In all the investigations mentioned above, the results were obtained from tests which were of relatively short duration. Even though inelastic deformation is known to be time dependent, most of the tests were conducted in conventional testing machines in which it was constantly necessary to adjust the head of the testing machine when loading in the inelastic range. The final deformation readings at each load were taken in all the investigations before a condition of equilibrium between time and deformation had been reached. The results, therefore, depend upon the duration of the test. In actual service the loads are not, in general, applied for short periods of time but rather are maintained at constant magnitude for extended periods of time.

In the present investigation service conditions were simulated by applying dead loads to the members for extended periods. To analyze the data a comparison was made of theoretical and experimental relations between a load parameter and deformation parameter in which each test load was maintained at a constant value until equilibrium was reached. The theoretical relations which were used in this comparison did not include time as a variable and the differences observed were attributed to time effects. The purpose of this investigation then was to present the experimental data for conventional short-time and for long-time dead-load tests of various ductile members, to compare theoretical and experimental results, and to attempt to explain differences observed between the two types of tests.

## 3. Scope

The main body of the bulletin is devoted to the presentation and analysis of test data concerning the load-carrying capacity of ductile beams as influenced by small amounts of inelastic action and by method and schedule of loading. These data were obtained from conventional tests made in screw- or hydraulic-powered testing machines as well as special tests made in a constant or dead-load testing machine.

A description is given of a series of tests made on straight and curved beams having various cross-sections and made from two types of materials.

* Parenthesized numbers refer to correspondingly numbered entries in the Bibliography.

Rectangular, circular, I-, and T-cross-section beams were investigated; the materials from which these beams were made were strain-hardening materials such as a high carbon steel and an aluminum alloy, and a non-strain-hardening material for small inelastic strains such as mild steel. The results of conventional short-time tests and the special dead-load tests are analyzed by comparing the experimental moment-strain and moment-deflection diagrams with those obtained by the usual theoretical considerations. In most instances there was good agreement between theory and experiment. The exceptions were the test results on the non-strain-hardening mild steel straight beams when tested under dead loading. For these beams the experimental moment-deformation diagrams fell appreciably below the theoretical curves, a fact that was attributed to the heterogeneous type of yielding which occurs in mild steel material during the yield point range of deformation.

To explain the disagreement between theory and experiment for members exhibiting heterogeneous yielding, special dead-load tests on tapered tension specimens were performed. The difference between the conventional lower yield point stress and that obtained by these dead-load tests of the tapered specimens was found to be sufficient to explain the disagreement in the results of the beam tests.

Although inelastic deformation is known to be a time-dependent phenomenon, the analyses used in most of the published data have not considered time as a variable. In this investigation it was found that the time effects of inelastic deformation were made visible or amplified when the members were subjected to constant or dead loads. The moment-deformation diagrams were found to have a stair-step appearance rather than the continuous form as usually reported. In some of the tests in which inelastic deformation had ceased at a given load, a delay of more than 30 min was observed before initiation of further inelastic deformation at an increased load. Furthermore, the time required for inelastic deformation to cease at a given load was found to be of several hours duration.

In Appendix A, a qualitative explanation of the observed time-dependent behavior is offered; it is based on considerations of the atomic, microscopic, and macroscopic levels of association of matter.

## 4. Acknowledgment

This investigation was conducted as a part of the work of the Engineering Experiment Station of the University of Illinois, of which Dean W. L. Everitt is the director, in the Department of Theoretical and Applied Mechanics, of which Professor T. J. Dolan is the head.

The curved beam analyses and tests were conducted by Professor Clark and Professor Corten under the direction of Professor J. O. Smith in satisfying the requirements for theses for degrees of Master of Science. Special acknowledgment is also due Professor J. O. Smith for his continued interest and helpful suggestions throughout the investigation and for his criticism of the manuscript.

## II. THEORETICAL MOMENT-DEFORMATION RELATIONS

This section presents the theoretical relationships between bending moment and strain in the most strained fibers and between bending moment and maximum deflection for straight and curved beams of various cross-sections. The results of four moment-strain derivations are contained herein; namely, straight beam relations for rectangular, circular, and I-cross-sections and the curved beam relation for the rectangular cross-section. The complete derivation of the moment-strain relation for a curved beam of rectangular cross-section is given in Appendix B along with the results of similar derivations for curved beams having cross-sections made up of rectangular elements.

The theoretical relations will first be presented to show the effect of the shape of the member on the load-carrying capacity of both straight and curved beams. Secondly, the strain-hardening characteristics of the material and their effects on the load-carrying capacity of a beam will be considered.

### 5. Assumptions Made and Method of Approach

The theoretical relations presented here are based on several assumptions. The material is assumed to be homogeneous and isotropic with identical properties in tension and compression. The beams are assumed to be subjected to a pure bending loading with the plane of the loading couples coinciding with one plane of symmetry of the beam cross-section.

It is further assumed that the total strain in any fiber of the beam is directly proportional to the distance of the fiber from the neutral surface. (This neutral surface, while stationary in the elastic range, may change in position due to inelastic action.) This assumption that plane sections remain plane after bending has been shown to be valid, at least statistically, for most solid-type cross-sections. However, for curved beams having flanged-type cross-sections of certain proportions, two investigations[12, 13] have shown it to be invalid. The further assumption is made that any fiber in the beam yields or that inelastic action is initiated when the stress in that fiber reaches the yield point of the material as determined from the conventional tension or compression tests; the justification of this assumption is given in Reference 7.

To facilitate the derivation of the moment-strain relation, the stress-strain diagram for the material is idealized by two straight lines as indicated by curve $OAB$ in Fig. 1. The straight line in the elastic portion has a slope equal to $E$, the modulus of elasticity of the material, while the slope in the inelastic portion is equal to $\alpha E$ where $\alpha$ may be considered to be the strain-hardening factor for the material. For many materials the stress-strain diagrams for tension and compression are not identical and would be represented by two idealized curves as shown in Fig. 1. In order to construct the moment-strain diagram within reasonable limits of accuracy, the average of these two curves, such as curve $OAB$, can be used for the idealization. For beams of rectangular cross-section, calculations indicate that for a 20 percent difference in yield strengths in tension and compression and $\alpha_1$ equal to $\alpha_2$, the error in the moment based on the average stress-strain diagram is less than 2 percent.

The theoretical moment-strain relations are obtained from the application of the basic equations of equilibrium to a free body diagram of a section of the loaded beam. The first of the two equations can be written

$$\int \sigma \, da = 0 \tag{1}$$

and states that the algebraic sum of all the resisting forces acting on the cut section of the cross-section must be equal to zero. This equation is used to locate the neutral axis of the beam. The second equilibrium equation can be written

$$\int (\sigma \, da) \, y = M \tag{2}$$

and states that the algebraic sum of all the moments of the external forces about any axis is equal to the resisting moment of the internal forces on the cut section about the same axis. The integral in Eq. 2 is evaluated by using the idealized stress-strain diagrams and the assumption concerning plane sections of the beam remaining plane after

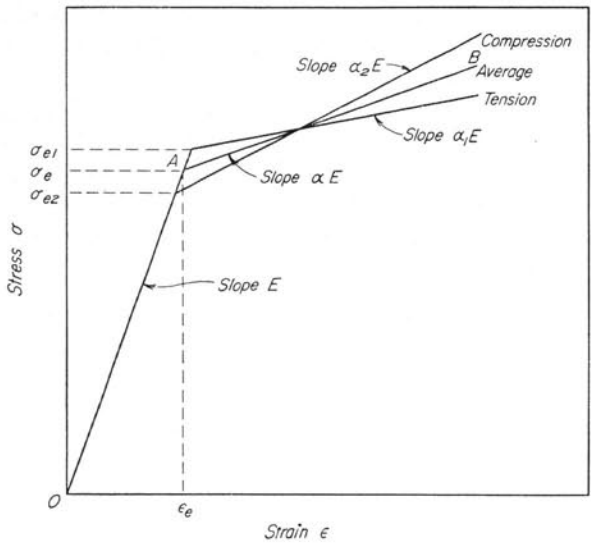


*Fig. 1. Idealized Tension and Compression Stress-Strain Diagrams and the Average Diagram*

bending. The equation which results is the moment-strain relation.

### 6. Effect of Shape of Beam on the Moment-Strain Relation

The effect of shape of beam includes both the effect of curvature of the beam as well as the effect of shape of the cross-section of the beam. The moment-strain relations that are presented to show the effect of shape were derived for a material with a flat-topped stress-strain diagram, i.e., one with a definite yield point ($\alpha = 0$ in Fig. 1).

*a. Effect of Curvature.* The effect of curvature of the beam will first be considered by presenting the results of several moment-strain relation derivations. Morkovin and Sidebottom[7] have derived the dimensionless moment-strain relation for a straight beam of rectangular cross-section. The expression can be written as follows

$$\frac{M}{M_e} = \frac{3}{2} - \frac{1}{2\lambda^2} \tag{3}$$

in which $\lambda = \epsilon_1/\epsilon_e$, $M_e$ is the maximum elastic resisting moment corresponding to a strain $\epsilon_e$ in the most strained fibers, and $M$ is the resisting moment corresponding to an inelastic strain $\epsilon_1$ in the most strained fibers of the beam.

The relation that corresponds to this equation for a beam of some definite curvature becomes more complicated since the stress distribution is not symmetrical with respect to the neutral axis and also since the neutral axis shifts with inelastic deformation. The derivation of the moment-strain

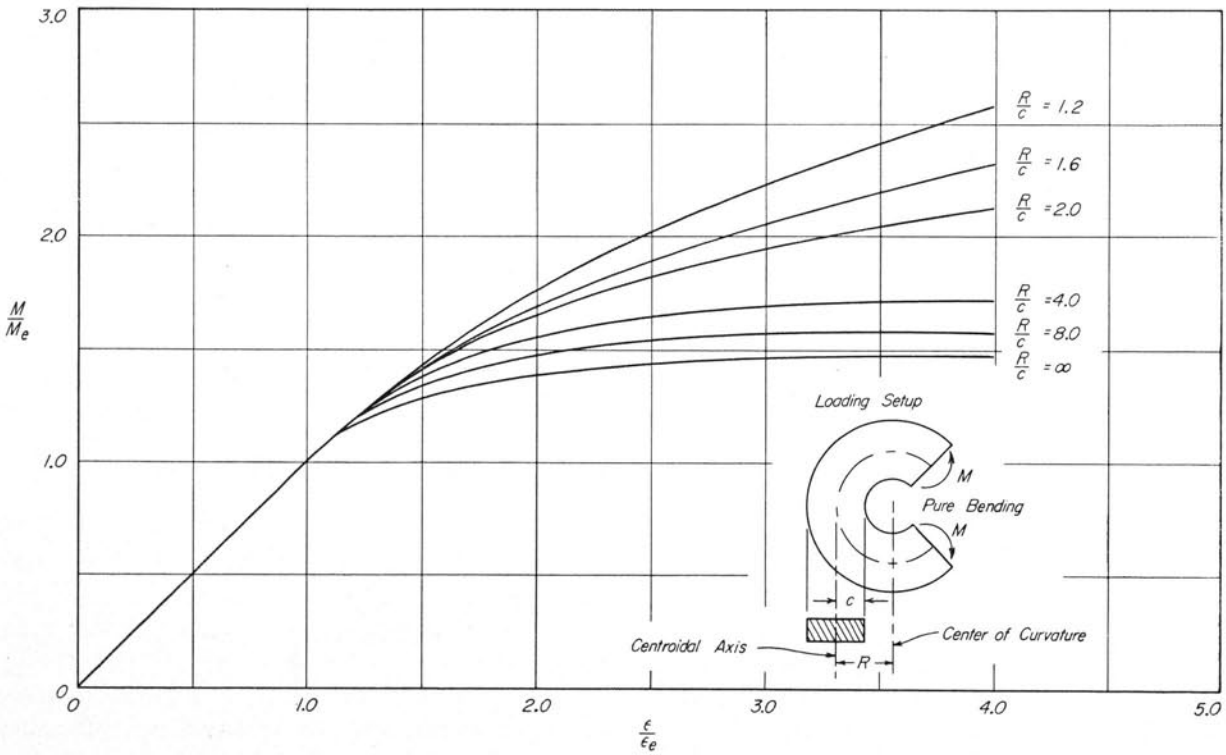


*Fig. 2. Theoretical Dimensionless Moment-Strain Diagrams for Curved Beams of Rectangular Cross-Section Showing Effect of Beam Curvature*

relation for a curved beam of rectangular cross-section is given in Appendix B. Two equations result from this derivation, one to locate the neutral axis and one to give the moment-strain relation, as follows:

$$\frac{1}{\lambda + \frac{\lambda}{n_1}} + \frac{n_2}{1 - n_2} + \ln\left(\frac{1 - n_2}{1 + \frac{n_1}{\lambda}}\right) = 0 \quad (4)$$

$$\frac{M}{M_e} = \frac{R_{na}{}^2 \lambda c_1'}{(\bar{R} - R_{na}')\, c_1\, (c_1' + c_2')} \left\{ \frac{-\left(2 + \frac{1}{n_1}\right)}{2\lambda \left(1 + \frac{1}{n_1}\right)^2} - \frac{1}{\frac{2\lambda}{n_1} + 2} + \frac{3n_2^2 - 2n_2}{2\,(1 - n_2)^2} + \ln\left(\frac{1 + \frac{n_1}{\lambda}}{1 - n_2}\right) \right\} \quad (5)$$

In these expressions $n_1$ equals $c_1/R_1$ and $n_2$ equals $c_2/R_2$ where $c_1$ and $c_2$ are distances from the neutral axis to inner and outer fibers of the beam for a given inelastic condition (see Fig. 32 in Appendix B) and $R_1$ and $R_2$ are the corresponding radii to inner and outer fibers of the beam. $R_{na}$ and $\bar{R}$ refer to the radius of curvature to the neutral axis and the centroid of the cross-section respectively. The prime on the symbol makes it refer to the elastic condition. Equations 4 and 5 are valid for a beam that yields only on the side containing the most strained fibers. The expressions for yielding on both sides of the beam are given in Appendix B.

The effect of curvature of the beam on the moment-strain relation is shown graphically in Fig. 2 for beams having rectangular cross-sections. The curves indicate that there is an increase in load-carrying capacity (i.e., the percentage increase in load above the elastic limit necessary to produce a given strain in the most strained fibers) when there is an increase in the curvature of the beam.

*b. Effect of Shape of Cross-Section.* The shape of the cross-section also has a decided influence on the increase in load-carrying capacity of a beam resulting from a given inelastic deformation. In addition to beams having rectangular cross-sections, relations have been derived for straight and curved beams with circular and I-cross-sections. The dimensionless moment-strain relation for a straight beam of circular cross-section as derived by Morkovin and Sidebottom[7] is:

$$\frac{M}{M_e} = \frac{1}{\pi}\left\{\frac{4}{3}\left(1 - \frac{1}{\lambda^2}\right)^{\frac{3}{2}} + 2\left(1 - \frac{1}{\lambda^2}\right)^{\frac{1}{2}} + 2\lambda \sin^{-1}\frac{1}{\lambda}\right\} \quad (6)$$

Two expressions were derived for a straight beam with an I-cross-section. The first equation can be written

$$\frac{M}{M_e} = \frac{1}{1 - B^3 + AB^3}\left\{\frac{3}{2} - \frac{1}{2\lambda^2} + B^3 (A - 1)\,\lambda\right\} \quad (7)$$

and is valid for yielding confined to the flanges of the beam. The second equation is

$$\frac{M}{M_e} = \frac{1}{1 - B^3 + AB^3}\left\{\frac{3}{2}(1 - B^2 + AB^2) - \frac{A}{2\lambda^2}\right\} \quad (8)$$

which is valid when yielding penetrates through the flanges into the web. In Equations 7 and 8, $A$ is the ratio of the thickness of the web to width of flange, and $B$ is the ratio of the depth of the beam to the distance between the inner faces of the flanges.

The effect of beam cross-section on the moment-strain relation for straight beams is shown graphically in Fig. 3. It should be noted that the I-beam, which was designed to have the greatest elastic flexural strength for a given weight of material, has the smallest increase in load-carrying capacity resulting from inelastic deformation.

Since several rather complex equations are required to construct the dimensionless moment-strain diagrams for curved beams with I- and T-cross-sections, these equations are listed in Appendix B. The effect of beam cross-section on the moment-strain relations for curved beams is shown graphically in Fig. 4.

### 7. Effect of Strain-Hardening on the Moment-Strain Relation

The dimensionless moment-strain relations which are plotted in Figs. 2, 3, and 4 were derived for a material such as mild steel which does not exhibit any strain-hardening for small inelastic strains.

If the material strain-hardens, the straight line $AB$ in Fig. 1 has a slope $\alpha E$ where $\alpha$ may be considered as a strain-hardening factor. The moment-

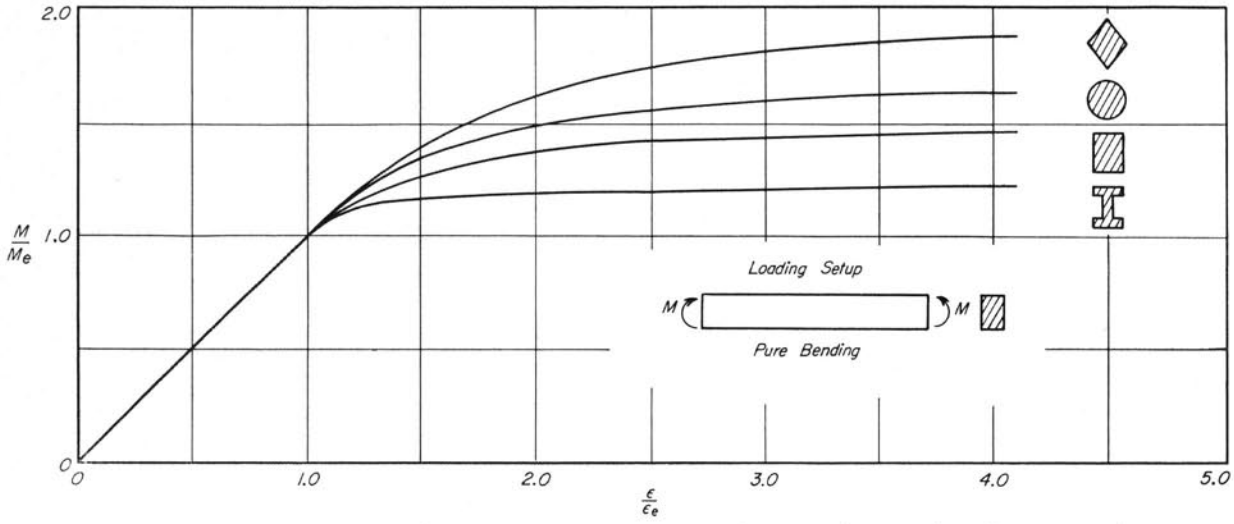


*Fig. 3. Theoretical Dimensionless Moment-Strain Diagrams for Straight Beams Showing Effect of Beam Cross-Section*

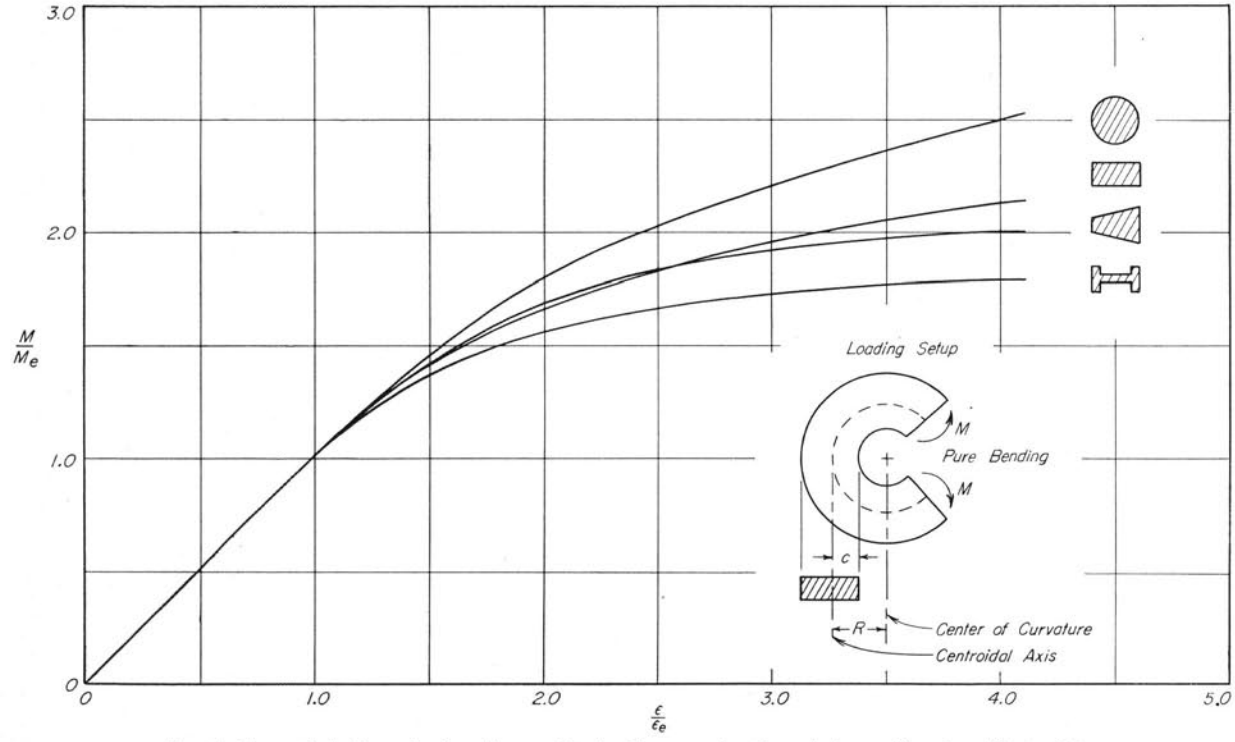


*Fig. 4. Theoretical Dimensionless Moment-Strain Diagrams for Curved Beams Showing Effect of Beam Cross-Section with the R/c Ratio Constant at 2.00*

strain relation and, hence, the load-carrying capacity for a given beam is greatly influenced by the magnitude of $\alpha$. A convenient method for introducing the strain-hardening effect into the moment-strain relations, developed on the assumption of no strain-hardening effect, is by means of the following equation:

$$\left.\frac{M}{M_e}\right]_{\alpha=\alpha_1} = \left.\frac{M}{M_e}\right]_{\alpha=0} + \alpha_1 \left\{\lambda - \left.\frac{M}{M_e}\right]_{\alpha=0}\right\} \quad (9)$$

This equation states that the moment ratio for a particular value of the strain ratio $\lambda = \epsilon_1/\epsilon_e$ and for any value of $\alpha$ is equal to the moment ratio for an $\alpha$ equal to zero plus the difference between the strain ratio $\lambda$ and the moment ratio for an $\alpha$ equal to zero mulitplied by the value of $\alpha$ for the material being considered. Equation 9 is exact for straight beams having cross-sections with two principal axes of symmetry. The equation is only

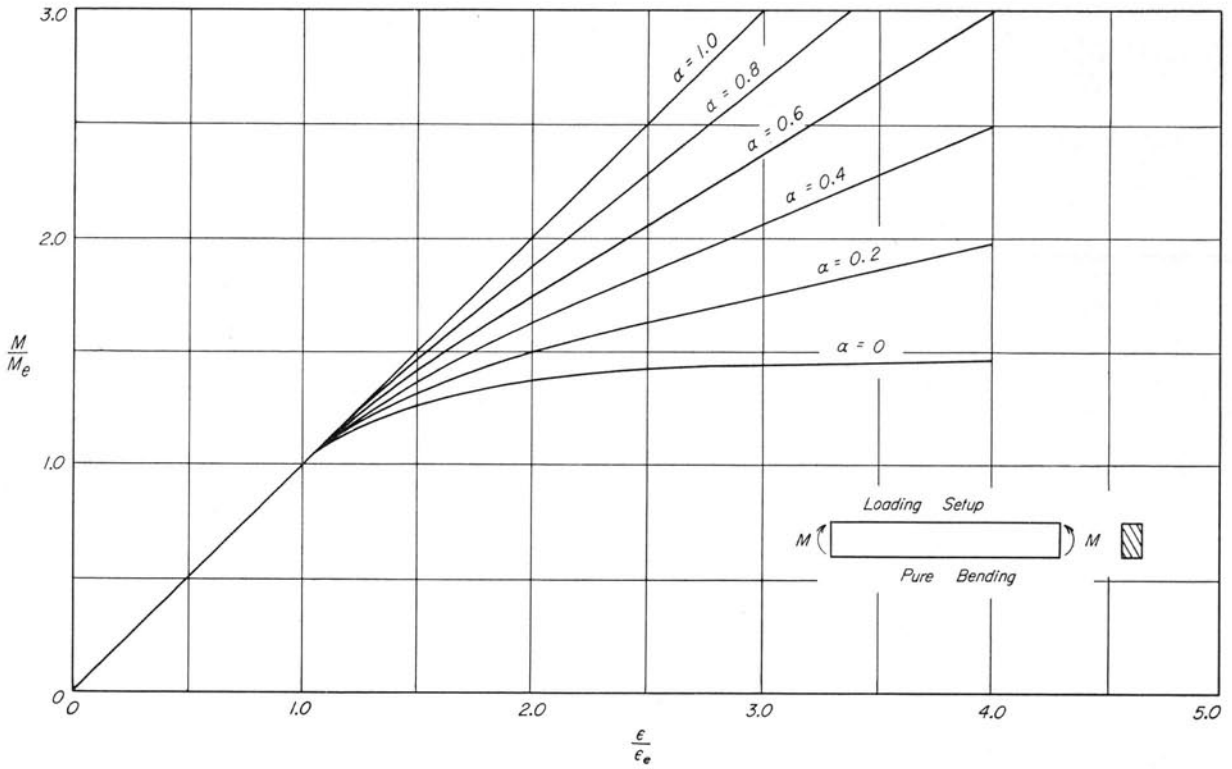


*Fig. 5. Theoretical Dimensionless Moment-Strain Diagrams for a Straight Beam of Rectangular Cross-Section Showing Effect of the Strain-Hardening Characteristic α*

approximate for curved beams since the neutral axis shifts with the inelastic deformation; however, the error is small (less than 5 percent) for all cases that have been investigated. The effect of strain-hardening on the dimensionless moment-strain relation for a straight beam of rectangular cross-section is shown graphically in Fig. 5.

## 8. Moment-Deflection Relations

In order to determine the deflection of a beam, it is necessary to determine the curvature at each section along the length of the beam. The curvature is proportional to the difference in strain in the most strained tension and compression fibers of the beam for either elastic or inelastic conditions. If the stress-strain diagrams of the material are the same for tension and compression, the curvature of the beam is proportional to the strain in the most strained tension or compression fibers for those cross-sections with two planes of symmetry. For this case the deflection of a statically determinate beam, which has been loaded beyond the elastic limit, can be obtained by the use of the moment-strain diagram with the procedure as outlined by Timoshenko.[14]

If a beam with the above limitations is subjected to pure bending, the moment-deflection diagram is identical with the moment-strain diagram, i.e.,

$$\frac{\Delta}{\Delta_e} = \frac{\epsilon_1}{\epsilon_e} = \lambda \qquad (10)$$

where $\Delta$ is the maximum deflection of the beam and $\Delta_e$ is the maximum elastic value of $\Delta$.

# III. MATERIALS AND METHOD OF TESTING

## 9. Materials Used and Types of Loading

To investigate experimentally the load-carrying capacity of straight and curved beams, tests were conducted on members made from two different types of materials under two different types of loading. The two types of materials investigated were (a) those that exhibit no strain-hardening characteristics at small inelastic strains and (b) those that do exhibit strain-hardening characteristics. Tests were made on these two types of materials since the strain-hardening characteristics have a decided influence on the time-sensitive inelastic behavior under load.

Mild steels from three different sources, with carbon content of approximately 0.2 percent, were chosen as representative of materials that do not strain-harden since these materials were found to have a definite yield point in the standard tension test. Material from the three different sources was investigated so that the observed behavior could not be attributed to any one heat of steel. A rail steel with a carbon content of approximately 0.8 percent and aluminum alloy 24S-T were taken to represent those materials that strain-harden from the onset of inelastic deformation. All of the steels were tested in the annealed condition.

One series of tests was conducted in the conventional screw-powered testing machine, each test being completed in a matter of several hours. Another series of tests was conducted in a dead-load testing machine where each test was continued over a period of several days, any particular load in the inelastic range being sustained until all inelastic deformation had apparently ceased. In the series of short-time tests in conventional testing machines, the load was applied in increments, and readings of load and deformation were taken immediately after application of the load. At loads which produced inelastic strains, the load was not maintained at a constant value until equilibrium was reached. In fact, for the larger loads, inelastic deformation continued to take place while the readings were being taken, even though the load was continually decreasing due to the inelastic deformation.

In the series of long-time tests, the beams were loaded in the dead-load testing machine pictured in Fig. 6. By means of the weights shown, any increment of dead load could be applied directly to the beam specimen. The testing procedure in these tests was as follows: Several loads were applied which resulted in elastic response, so that the elastic behavior of the beam was obtained. For inelastic load applications, the nuts on the safety rods were first adjusted so that any additional load was carried by these rods. Then the proper load increment was applied by adding weights on the load rig, and the nuts on the safety rods were loosened. In this manner the increment of load was applied to the beam during the time interval necessary to loosen the safey rod nuts, a period of some 5 to 30 sec depending on the magnitude of the load increment. A large spring was also incorporated into the rig where the main loading rod was attached to the weights in order to further insure a smooth application of the load. Deformation readings were taken immediately upon the application of each increment of load and at intervals of time until inelastic deformation ceased at that load. Usually the inelastic deformation at a given load ceased after 6 hr, but observations were continued and another increment was not applied until 12 to 72 hr had elapsed.

## 10. Test Specimens and Deformation Measurements

Tests on non-strain-hardening materials included mild steel straight beams of rectangular, circular, and I-cross-sections and mild steel curved beams with rectangular, I-, and T-cross-sections. Tests made on strain-hardening materials included straight and curved rail steel beams and a straight beam of 24S-T aluminum alloy, all having rectangular cross-sections. These beams are all listed in Table 1 along with other pertinent information which is explained hereafter. Numbers 1 through 9 designate straight beams and 10 through 15 curved beams. The letter following the beam number refers to the type of testing machine used, S designating the short-time test in a screw-powered machine and L the long-time test in the dead-load machine.

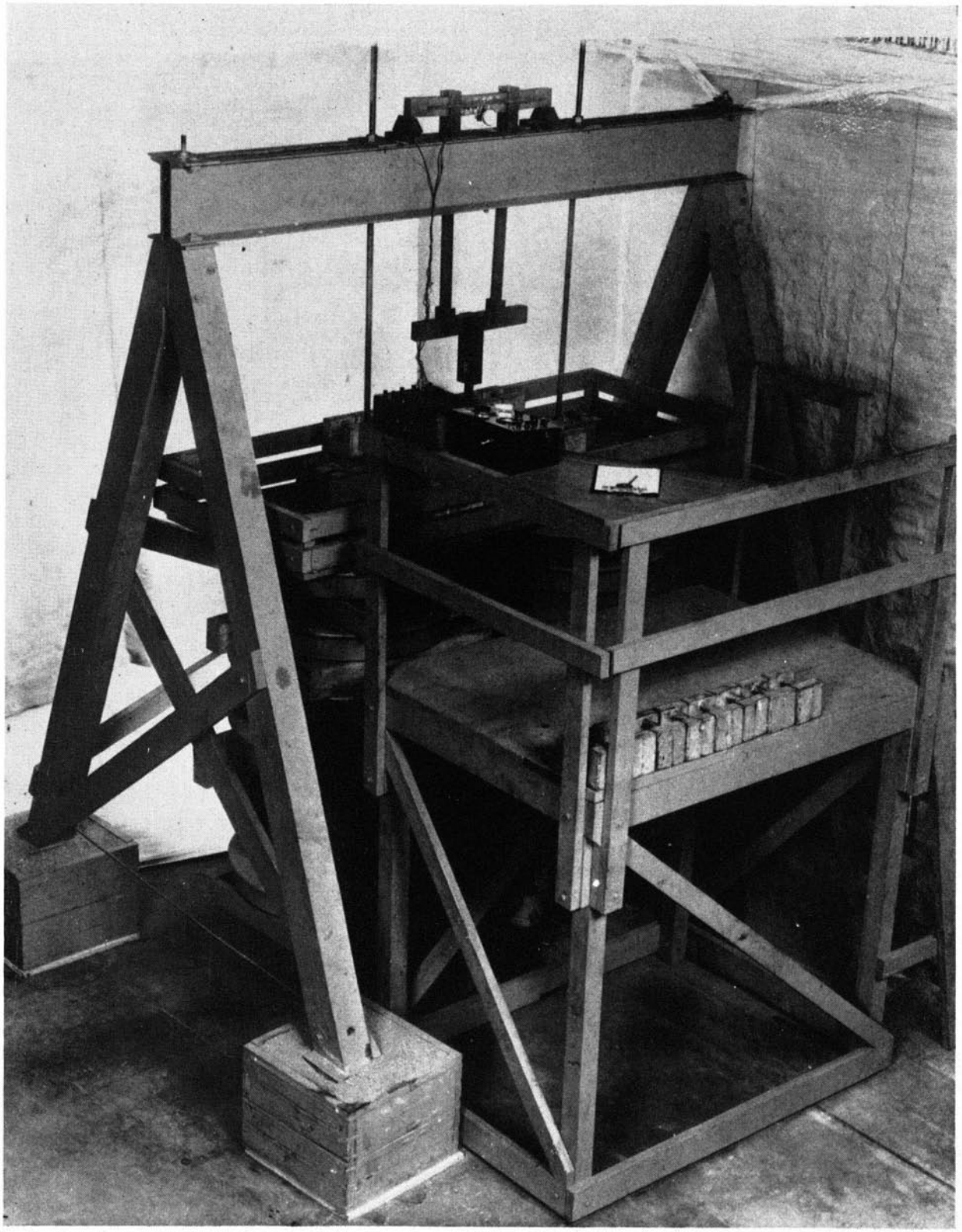

*Fig. 6. Dead-Load Testing Machine*

Table 1

Types and Dimensions of Beams, Methods of Loading, and Properties of Materials

STRAIGHT BEAMS

| Beam Designation | | 1-S | 2-L | 3-S | 4-L & 5-L | 6-L | 7-S & 8-L | 9-L |
|---|---|---|---|---|---|---|---|---|
| Cross-Sectional Dimensions | | 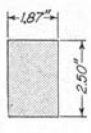  | 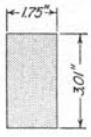  | 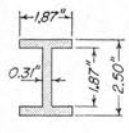  | 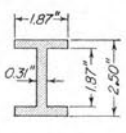  |   | 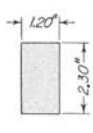  | 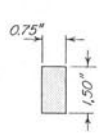  |
| Beam Dimensions | $l$, in. | 46 | 38.31 | 46 | 23 | 23 | 23 | 15.5 |
| | $a$, in. | 8 | 12.31 | 8 | 11 | 11 | 8 | 8 |
| | $b$, in. | 46 | 15.31 | 46 | 13.5 | 13.5 | 10.75 | 11 |
| Type of Loading | | Pure Bending | Pure Bending | Pure Bending | Pure Bending | Pure Bending | Pure Bending | Pure Bending |
| Type of Machine | | Screw-Powered | Dead-Load | Screw-Powered | Dead-Load | Dead-Load | Screw-Powered | Dead-Load |
| Length of Test | | Short-Time | Long-Time | Short-Time | Long-Time | Long-Time | Short-Time Dead-Load Long-Time | Long-Time |
| Material | | Mild Steel | Annealed SAE 1020 Steel | Mild Steel | Annealed Mild Steel | Annealed Mild Steel | Annealed Rail Steel | Aluminum Alloy 24S-T |
| Properties of the Material | $\sigma_e$, psi | 27,700 | 28,100 | 27,700 | 28,400 | 30,100 | 38,400 | 47,500 |
| | $\epsilon_e$, in./in. | .00092 | .00094 | .00092 | .00095 | .00100 | .00127 | .00437 |
| | $\alpha$ | 0 | 0 | 0 | 0 | 0 | .081 | .085 |
| | $\Delta\sigma_e$, % | ±6.5 | ±3.0 | ±6.5 | ±4.0 | ±5.8 | ±5.9 | ±3.2 |
| | $N$ | 8 | 6 | 8 | 8 | 12 | 6 | 10 |

CURVED BEAMS

| Beam Designation | | 10-S | 11-L | 12-S | 13-L | 14-L | 15-S |
|---|---|---|---|---|---|---|---|
| Cross-Sectional Dimensions | | 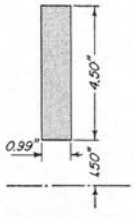  | 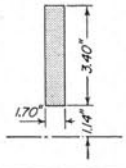  | 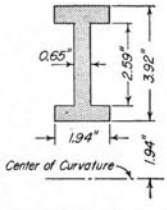  | 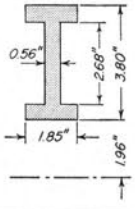  | 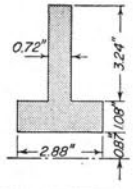  | 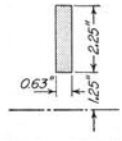  |
| Type of Loading | | Moment & Direct Load | Pure Bending | Moment & Direct Load | Moment & Direct Load | Moment & Direct Load | Moment & Direct Load |
| $d$, in. | | 10 | .. | 4.5 | 4.09 | 6.83 | 11.83 |
| $R/c$ Ratio | | 1.67 | 1.67 | 2.0 | 2.04 | 1.60 | 2.11 |
| Type of Machine | | Screw-Powered | Dead-Load | Screw-Powered | Dead-Load | Dead-Load | Screw-Powered |
| Length of Test | | Short-Time | Long-Time | Short-Time | Long-Time | Long-Time | Short-Time |
| Material | | Annealed Mild Steel | Annealed Mild Steel | Mild Steel | Annealed Mild Steel | Mild Steel | Rail Steel |
| Properties of the Material | $\sigma_e$, psi | 32,000 | 34,600 | 28,400 | 28,400 | 24,500 | 54,000 |
| | $\epsilon_e$, in./in. | .00112 | .00115 | .00096 | .00096 | .00083 | .00183 |
| | $\alpha$ | 0 | 0 | 0 | 0 | .035 | .0733 |
| | $\Delta\sigma_e$, % | ... | 1.7 | ... | ... | ... | ... |
| | $N$ | 3 | 6 | 2 | 2 | 2 | 3 |

All straight beams were subjected to two-point loading such as that shown in Fig. 7. This loading arrangement gave a test section of constant bending moment over the central portion of the beam of length $a$. The deflection was measured over the length of beam designated by $b$. The dimensions $a$ and $b$ as shown in Fig. 7 are listed in Table 1 for all straight beams. All of the curved beams except Beam 11L were loaded as shown in Fig. 8, the test section being subjected to a combination of bending moment and direct load. The moment arm, dimension $d$ in Fig. 8, is listed for each beam in Table 1. This dimension, in all cases, was large enough so that the direct stress for elastic conditions was less than 10 percent of the maximum bending stress. Beam 11L was subjected to a constant bending moment over the major portion of the beam by the loading arrangement shown in Fig. 9.

The deformation of each beam was obtained both by measuring the strains at various positions

across the depth of the test section and by measuring the deflection of the beam. The strains were measured by wire-type electrical resistance (SR-4) strain gages of various gage lengths. The deflection measurements were so taken as to check the readings of the SR-4 strain gages since there was some question as to the reliability of such gages held at large strains for extended periods of time. The test data indicate good agreement between the two

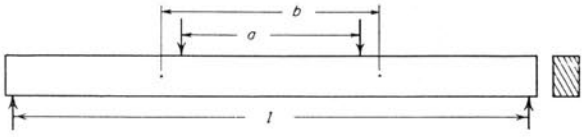


*Fig. 7. Loading Setup for Straight Beams*

methods of measurement; therefore it could be concluded that the cement bond between strain gage and specimen did not creep appreciably under sustained high strains.

The theoretical relations presented in Chapter II are based on the assumption that the strain distribution in the beam varies linearly across the depth of the beam. Although the heterogeneous yielding which occurs in mild steel does not warrant this assumption, previous investigations[7] indicate that the strain distribution in the beam does remain linear when the strains are measured over gage length sufficiently long to give a statistical average. In view of this, the gage lengths of the SR-4 gages were so chosen as to measure an average strain. The average strains in all the mild steel beams subjected to dead loading were measured by type A-9 gages having a gage length of 6 in. An investigation of the heterogeneous nature of the yielding in mild steel was made using type A-18 and A-7 gages with gage lengths of ⅛ and ¼ in. respectively on Beam 2L. The results of this investigation

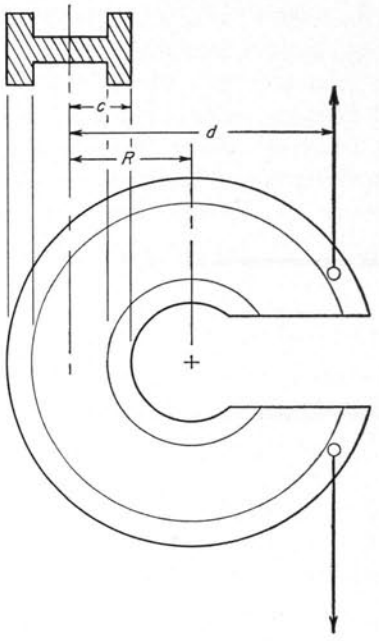


*Fig. 8. Loading Setup for Most of the Curved Beams*

are given in Chapter IV. For Beams 1S and 3S,[15] tested in a screw-powered machine, the average strains were measured by 1-in. gage length type A-11 SR-4 gages and checked by a special C-type gage having a 4-in. gage length.

For the rail steel and aluminum alloy straight beams, type A-11 SR-4 gages were used to measure the average strains in the most stressed fibers. Gages with shorter lengths were used to confirm the homogeneous nature of yielding in these materials. The average strains in the most stressed fibers of the curved beams were measured by type A-11 gages having the 1-in. gage length. Shorter length gages were used to check the strain distributions against the assumptions made in the theoretical derivations.

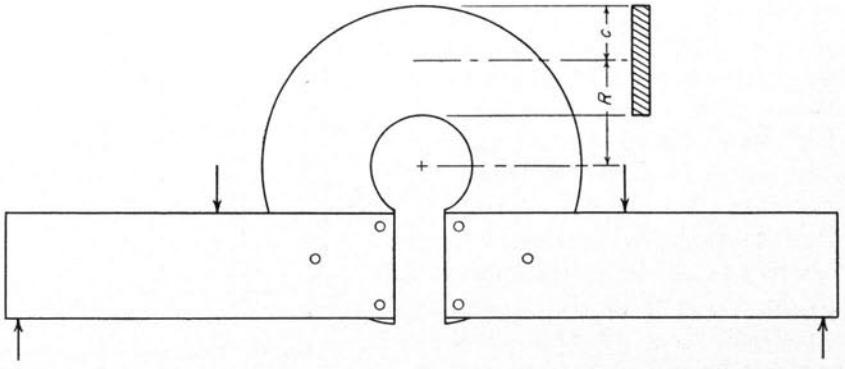


*Fig. 9. Loading Setup for Pure Bending of Curved Beam 11L*

The deflections of all beams, both straight and curved, were measured by a pair of 0.0001-in. dial gages, one mounted on either side of the beam in order to obtain an average reading. This arrangement was also used to detect the presence of unsymmetrical bending in the specimen. For the straight beams the deflection was measured over a length, represented by dimension $b$ in Fig. 7, which was a little greater than the length of the constant moment section of the beam. The dimension $b$ is listed in Table 1 for all beams. The deflection of the curved beams was measured on a diameter at the centroidal surface of the beam.

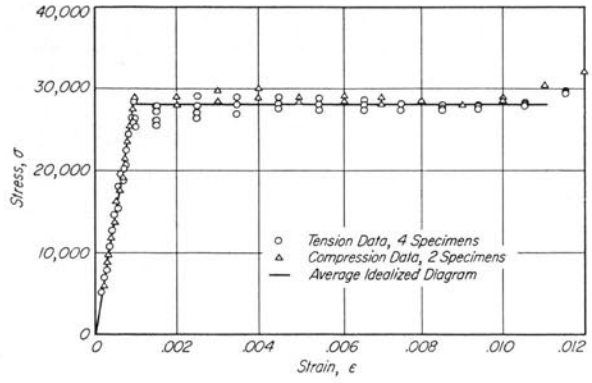


*Fig. 10. Stress-Strain Diagrams for Annealed SAE 1020 Steel*

### 11. Properties of the Materials

The properties of the materials which were required for an analysis of the experimental results are embodied in the shape of the stress-strain diagram in tension and compression for a range of strain up to 10 or 15 times the maximum elastic strain. To obtain these diagrams, tension and compression specimens were machined from the same bars of material from which the corresponding beam specimen was machined. The tension specimens were standard ½-in. diam round specimens having a 2-in. gage length for strain measurements, and the compression specimens were standard ¾-in. diam round specimens with a 1-in. gage length. Strains were measured by mechanical gages, and conventional testing procedures were followed in all the tests.

The data in these stress-strain diagrams were observed to have appreciable scatter. In view of this, additional diagrams were obtained from specimens taken from material as near as possible to the test section of the beam specimen. This was accomplished by cutting specimens from the portions of the beam specimen that had not been inelastically deformed. In some instances the variation of properties across the width and depth of the beam specimen was found by cutting rectangular tension specimens from the beam at various positions. These specimens had a cross-section ¾-in. wide and ¼-in. thick. The strains were measured using the same 2-in. extensometer as was employed in the standard tension tests. Self-aligning Templin grips were used to pull the specimens in tension.

All of the stress-strain diagrams in tension and compression obtained for the material used in mild steel Beam 2L are plotted in Fig. 10. The scatter of the data is evident, and these diagrams are typical of the other two mild steels which were investigated. The stress-strain diagrams in tension and compression for the material used in rail steel Beam 8L are shown in Fig. 11, and for the aluminum alloy material used in Beam 9L in Fig. 12. The strain-hardening characteristics of these two materials at small inelastic strains are evident in the diagrams.

As was discussed in Chapter II, the theoretical moment-strain relation is based on the assumption that the stress-strain relation can be represented by two straight lines as indicated in Fig. 1. In Figs. 10, 11, and 12 the idealized or average stress-strain diagrams are shown by the solid lines. The intersection of the two straight lines determines the

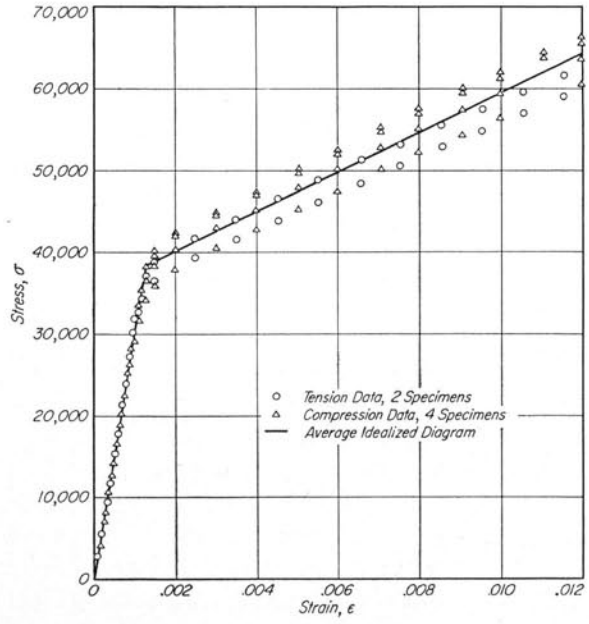


*Fig. 11. Stress-Strain Diagrams for Annealed 0.8 Percent Carbon (Rail) Steel*

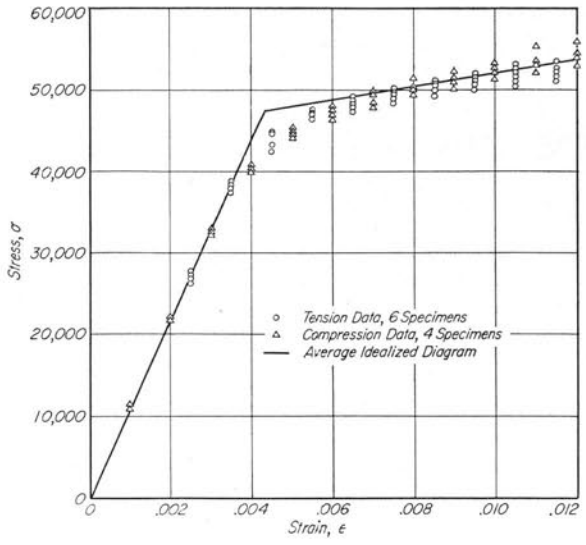


*Fig. 12. Stress-Strain Diagrams for As-Received 24S-T Aluminum Alloy*

magnitude of the yield stress $\sigma_e$ and the yield strain $\epsilon_e$. The slope of the line through the inelastic region gives $\alpha E$ from which the strain-hardening factor $\alpha$ can be determined. It was also mentioned in Chapter II that the theoretical relations were derived on the assumption of identical properties in tension and compression. Although this assumption is not valid for the aluminum alloy, the average stress-strain diagram was found to introduce a very small error in constructing the theoretical moment-deformation diagrams.

In Table 1 the quantities $\sigma_e$, $\epsilon_e$, and $\alpha$ are listed for the materials used in making the beam specimens. An indication of the variation of the stress-strain properties is given by the quantity $\Delta\sigma_e$ which is the range of variation of the yield stress obtained from the various specimens in both tension and compression; $N$ is the number of tension and compression specimens tested for the material.

# IV. PRESENTATION AND ANALYSIS OF EXPERIMENTAL DATA

In Chapter II theoretical dimensionless moment-deformation relations (Eq. 1 through 10) were presented for straight and curved beams of various cross-sections. In order to determine the validity of these theoretical relations, tests were conducted on straight and curved beams having various cross-sections and made of various materials. In the following sections, comparisons will be made between the theoretical relations and test data obtained from dead-load tests and, in most cases, short-time tests.

Inelastic deformation is known to be a time-dependent phenomenon; however, most of the investigators who have reported data obtained from short-time tests have not included this variable in the analysis of their results. The testing under dead loads accentuated the time effects, and the test results exhibit peculiarities which have not been de-

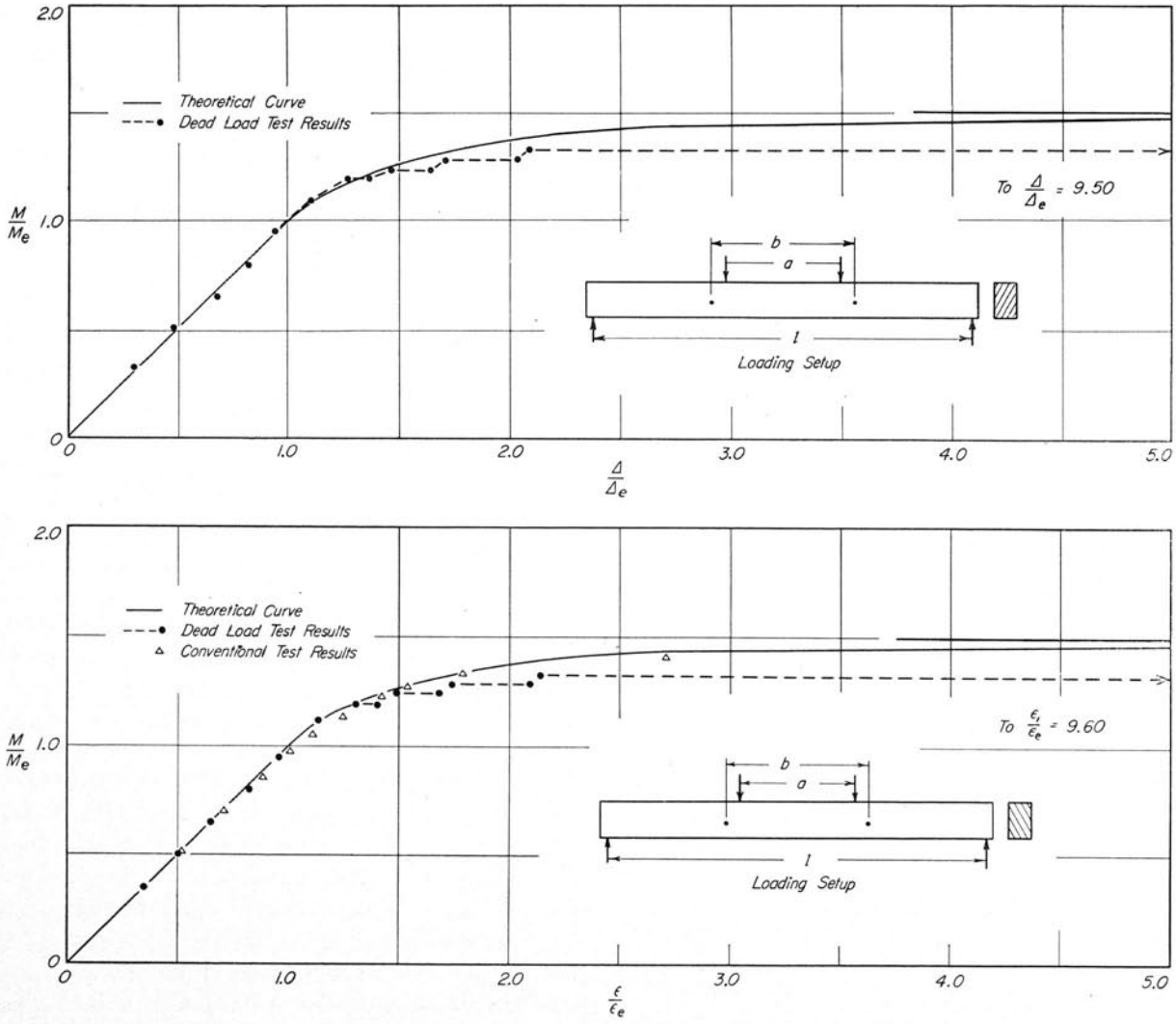


*Fig. 13. Dimensionless Moment-Deformation Diagrams for Mild Steel Straight Beams 1-S and 2-L Having Rectangular Cross-Sections*

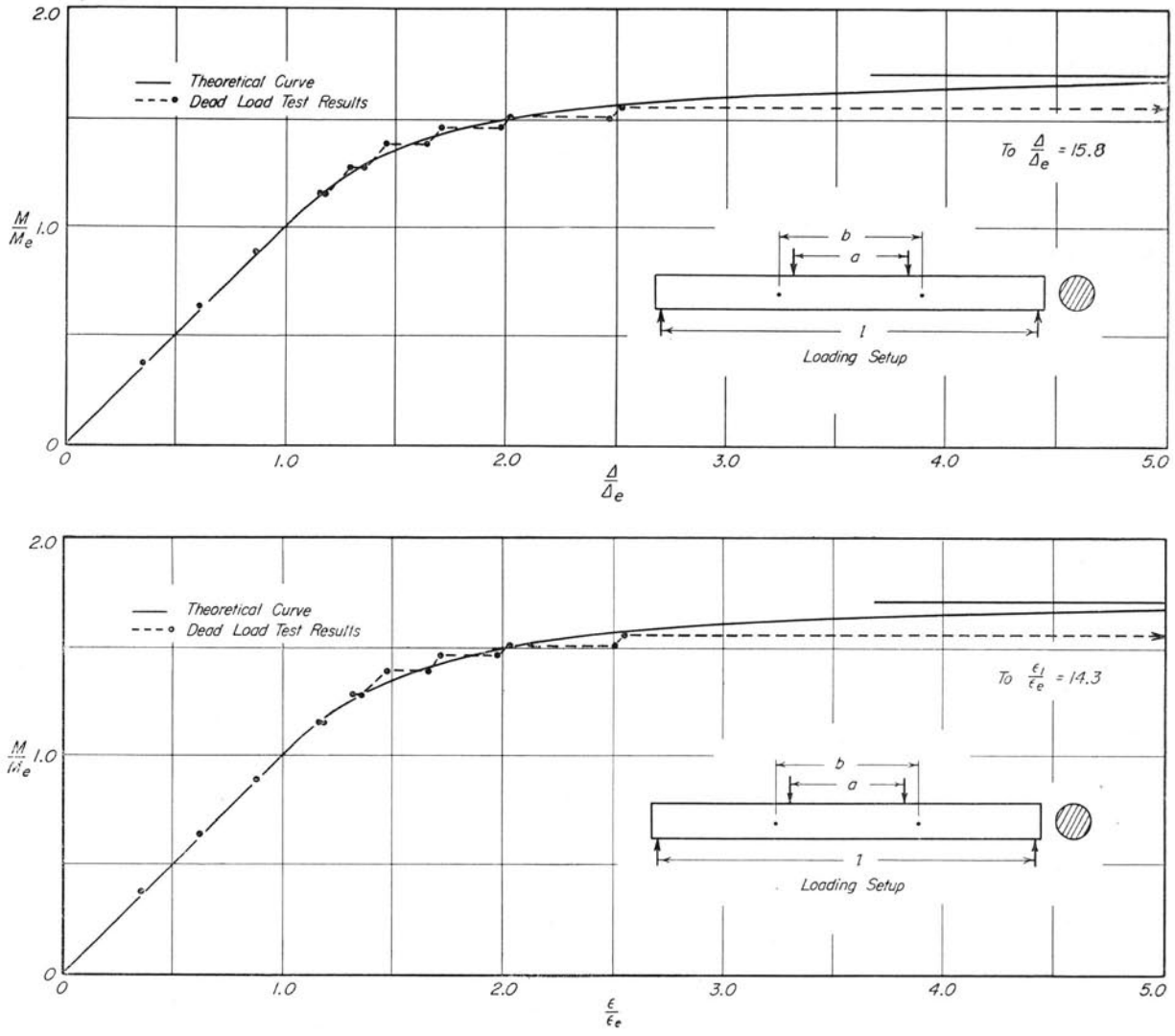


*Fig. 14. Dimensionless Moment-Deformation Diagrams for Mild Steel Straight Beam 6-L Having a Circular Cross-Section*

scribed fully in the literature. These peculiarities will be discussed following the presentation of the data.

### 12. Results for Straight Beams Made of Non-Strain-Hardening Materials

One rectangular section beam, one circular section beam, and two I-section beams all made from mild steels having definite yield points were subjected to dead-load tests. The theoretical dimensionless moment-strain curves for these beams are shown in the lower graphs in Figs. 13, 14, and 15, and the theoretical curves are represented by the solid lines. The curve as plotted in Fig. 13 for the rectangular section beam was obtained using Eq. 3. In Fig. 14, Eq. 6 was used to obtain the curve for the mild steel beam of circular cross-section, and Fig. 15 shows the curves obtained for the I-section beam using Eqs. 7 and 8 when constants $A$ and $B$ have values of 0.166 and 1.336, respectively.

The theoretical dimensionless moment-deflection curves, shown in the upper graphs in Figs. 13, 14, and 15, were obtained by assuming that $\Delta/\Delta_e$ was equal to $\epsilon_1/\epsilon_e$; therefore these curves are identical with the theoretical moment-strain curves. This assumption is valid only in case the deflection is computed for a length of the beam subjected to a constant moment section. As indicated in Fig. 7 and listed in Table 1, the length $b$ over which the deflection was measured was slightly longer than the constant moment section $a$; however, the above assumption introduced an error in each case of less than 1 percent.

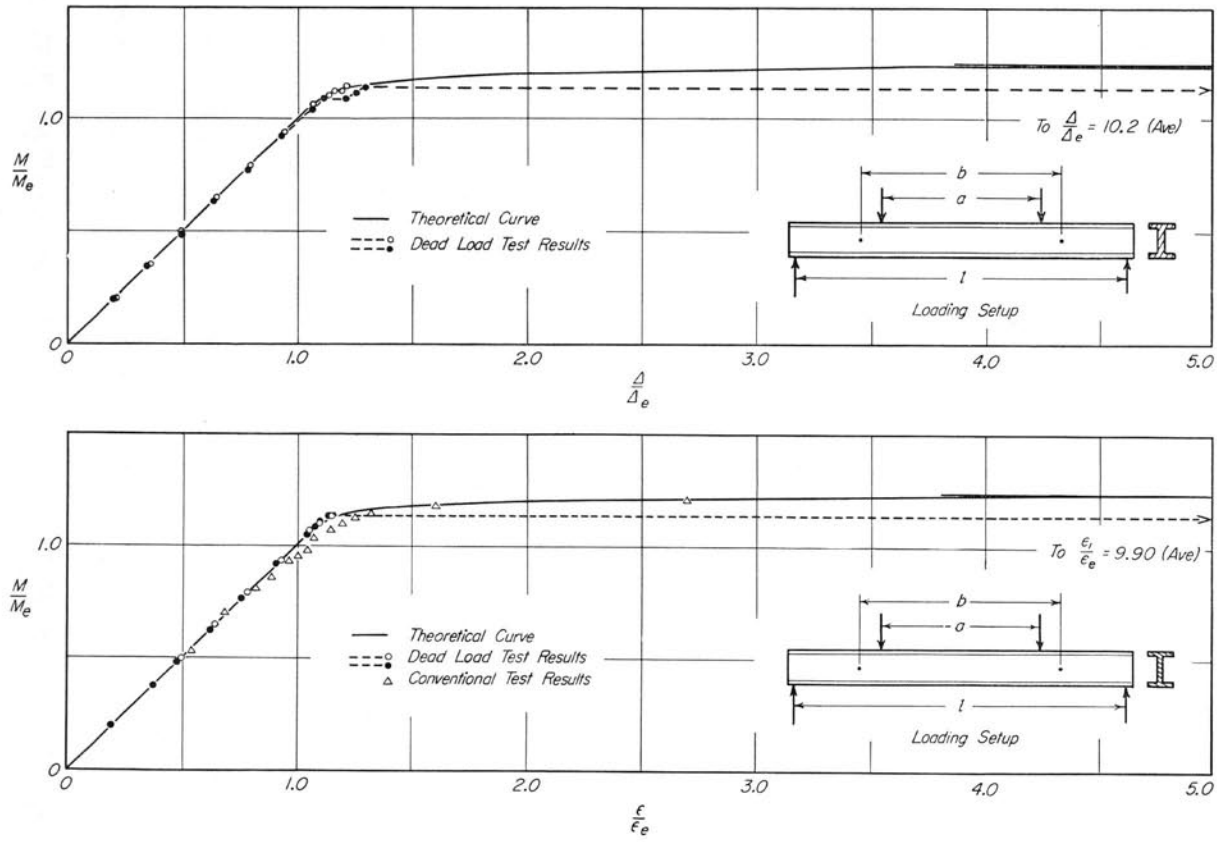


*Fig. 15. Dimensionless Moment-Deformation Diagrams for Mild Steel Straight Beams 3-S, 4-L, and 5-L Having I-Cross-Sections*

In all of the beam tests strain in the extreme fibers and deflection of the central portion of the beam were measured at each of the various increments of load. For dead-load testing, these readings, at loads which produced inelastic deformation, were taken immediately after the load was applied and at various intervals until deformation ceased. For each load the bending moment was calculated and divided by the maximum elastic moment, $M_e$, and the strain and deflection for the beginning and end of each deformation period were divided by $\epsilon_e$ and $\Delta_e$, respectively, the maximum elastic strain and deflection. In Figs. 13, 14, and 15 these dead-load test points for the various beams are plotted as solid and open circles and are connected by dashed lines.

As previously stated, tests were also made on beams in the conventional screw-powered or hydraulic testing machine where the tests were completed in a relatively short period of time. For comparison with the theoretical curves and the results from the dead-load tests, moment-strain data are also shown in Figs. 13 and 15 for beams of rectangular and I-cross-sections obtained from the conventional method of testing. These data are plotted as open triangles and are typical of those reported by other investigators.[7, 15]

The experimental moment-deformation data usually reported for these short-time tests follows a continuous curve and either checks the theoretical curve or is found to lie above it. In contrast to these results, the diagrams for the dead-load tests were found not to be continuous but to have a stair-step appearance. As shown in Figs. 13, 14, and 15 the dead-load test points fell considerably below the theoretical curves for the larger values of inelastic strain. Equations 3, 6, and 8 indicate that the theoretical curves have a horizontal asymptote for large inelastic strains. The resisting moment corresponding to this asymptote is generally referred to as the fully plastic moment or the moment corresponding to a plastic hinge. In Figs. 13, 14, and 15 this fully plastic moment is shown as the solid horizontal line. The uppermost horizontal dashed line for each of the experimental curves represents the experimentally-determined hinge moment, i.e., the moment at which excessive deformation occurs at constant load. The numbers at the ends of these lines give the magnitude of the

strain and deflection ratio when yielding had ceased at the experimental hinge moment.

Consider the dead-load test data in terms of the difference between the maximum plastic and elastic moments. Theoretically these differences should be $0.70M/M_e$, $0.50M/M_e$, and $0.23M/M_e$ for beams of circular, rectangular, and I-cross-sections, respectively. The corresponding difference between the experimental hinge values and the elastic moments were found to be $0.52M/M_e$, $0.33M/M_e$, and $0.16M/M_e$ or only 74, 66, and 70 percent of the theoretical values. In contrast to the dead-load test data, the data obtained from short time tests have been found to check the theoretical values very closely. Since many service applications involve constant loads of long duration, it would seem necessary to account for the differences observed. This reduction can be explained by considering the non-homogeneous nature of yielding in mild steel members; the information is presented in Section 15, and Appendix A.

### 13. Results for Straight Beams Made of Strain-Hardening Materials

Only beams of rectangular cross-section were tested in the investigation of materials which strain-harden. Annealed rail steel (carbon content—approximately 0.8 percent) and 24S-T aluminum alloy were the materials used in making the beams. The test results are shown for rail steel beams 7-S and 8-L in Fig. 16 and for aluminum alloy beam 9-L in Fig. 17. The theoretical dimensionless moment-strain curves for the beams were obtained using Eqs. 3 and 9 with $\alpha$ equal to 0.081 for the rail steel and 0.085 for the aluminum alloy. Follow-

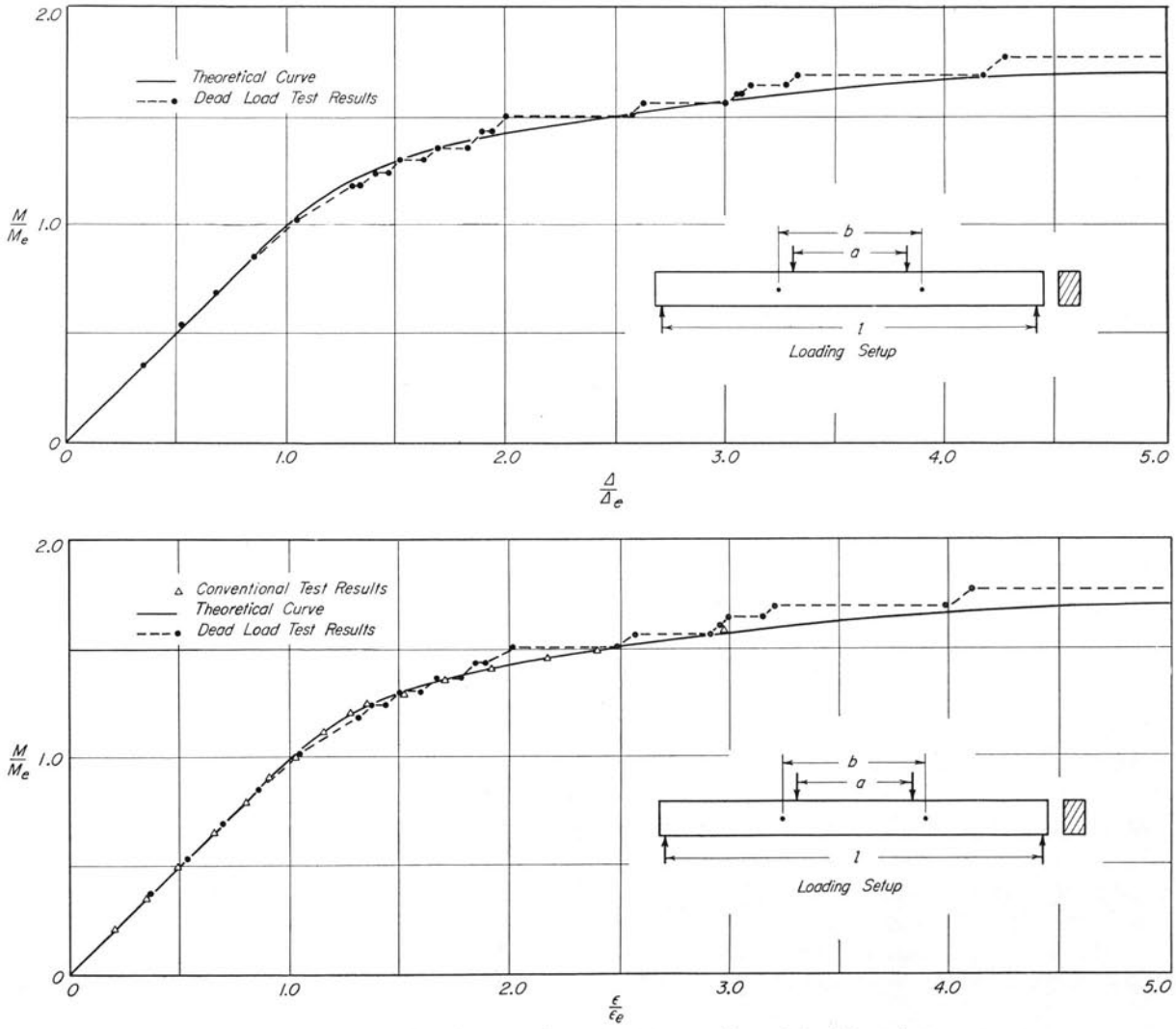


*Fig. 16. Dimensionless Moment-Deformation Diagrams for Rail Steel Straight Beams 7-S and 8-L Having Rectangular Cross-Sections*

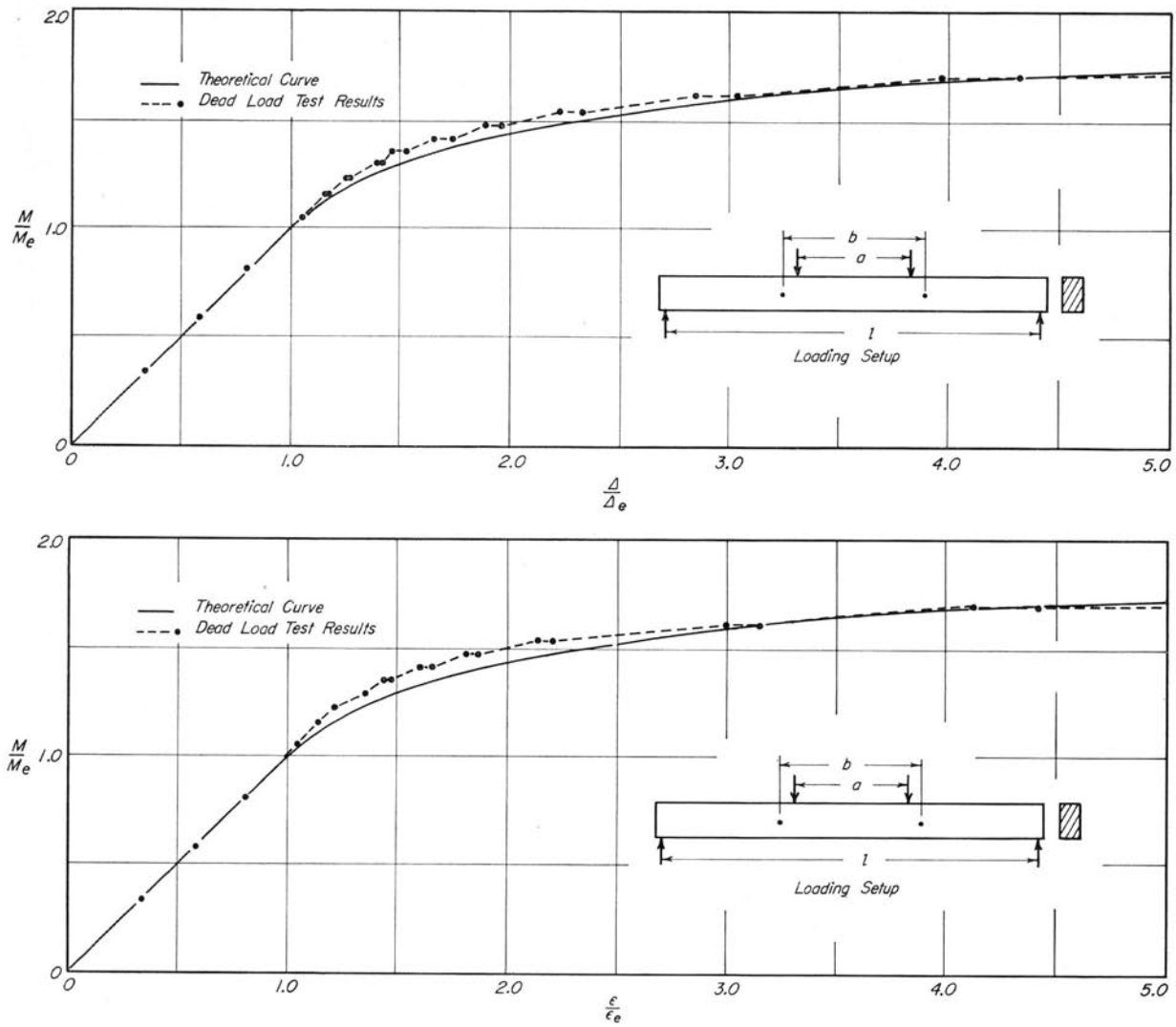


*Fig. 17. Dimensionless Moment-Deformation Diagrams for Aluminum Alloy 24ST Straight Beam 9-L Having a Rectangular Cross-Section*

ing the method as outlined in Section 8, the idealized average diagram was used in plotting the theoretical moment-strain curve for the aluminum alloy. As was done for the mild steel beams, the moment-deflection curves were obtained by setting $\epsilon_1/\epsilon_e$ equal to $\Delta/\Delta_e$. The experimental moment-deformation data for the dead-load tests of these two strain-hardening materials are plotted in Figs. 16 and 17 as solid circles joined by dashed lines. In contrast to the mild steel beams the test points for these beams were found to lie either on or above the theoretical curves. The data for the rail steel beam exhibited the same stair-step appearance as did the mild steel beams, but the diagrams for the aluminum alloy beam were almost continuous curves. In all the steel beam tests any additional load increment resulted in elastic response before the inelastic deformation took place. In the aluminum alloy beam test the additional load caused immediate deformation in which the elastic and plastic components could not be distinguished in the loading phase.

### 14. Results for Curved Beams

Three curved beams, one each of rectangular, I-, and T-cross-sections, were subjected to dead-load testing. The results for these beams are shown in Figs. 18, 19, and 20. The theoretical dimensionless moment-strain curve for the beam of rectangular cross-section, shown as the solid line in Fig. 18, was obtained using Eqs. 4 and 5 for yielding at

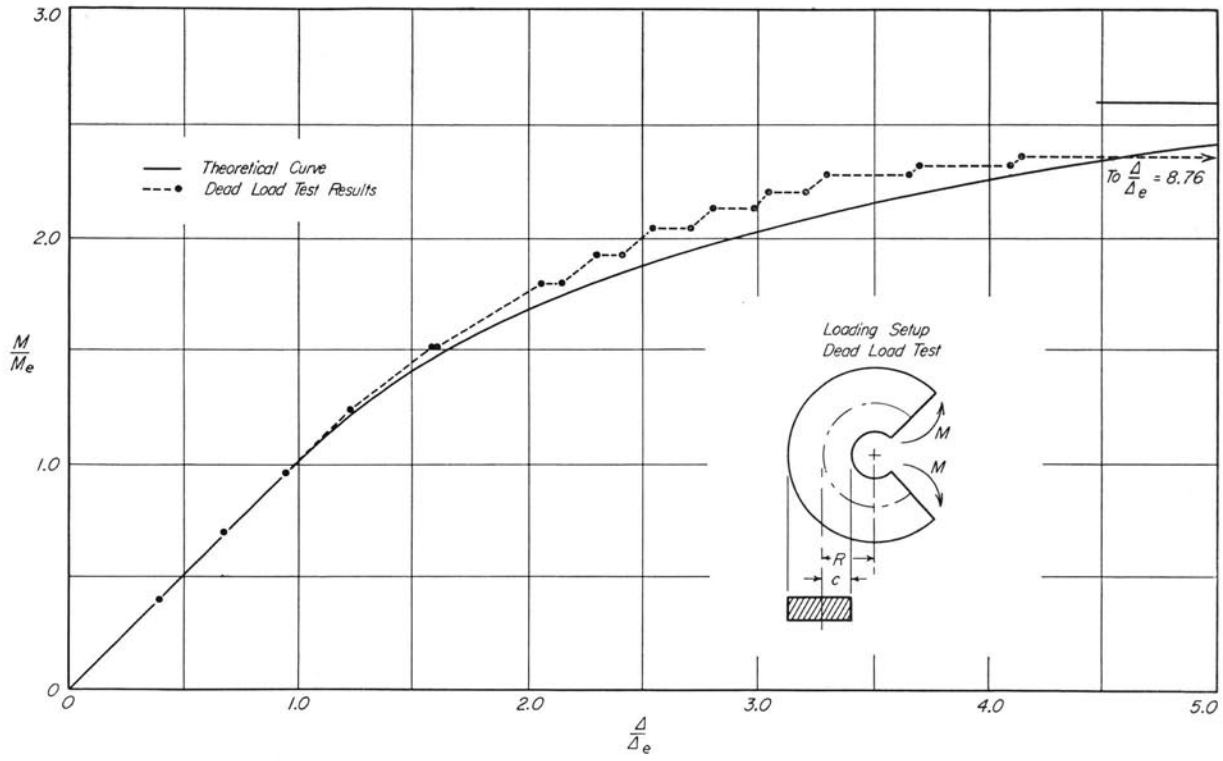


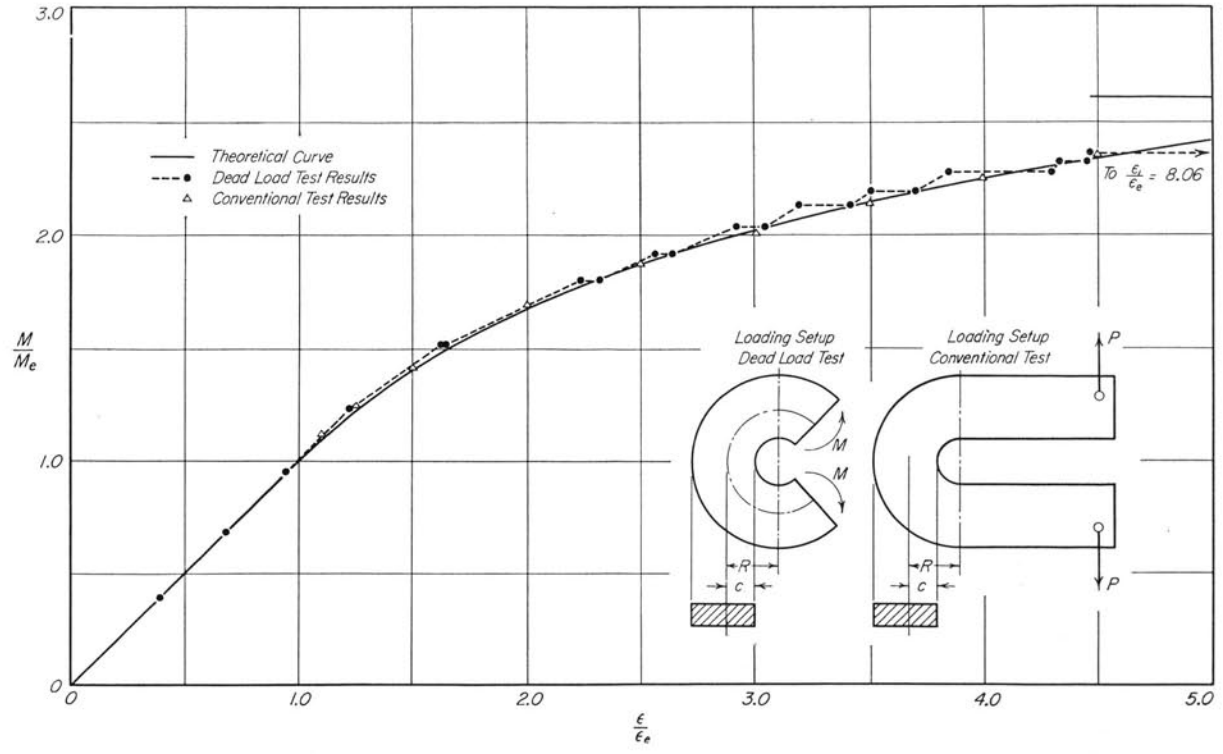


*Fig. 18. Dimensionless Moment-Deformation Diagrams for Mild Steel Curved Beams 10-S and 11-L Having Rectangular Cross-Sections. R/c Ratio = 1.67*

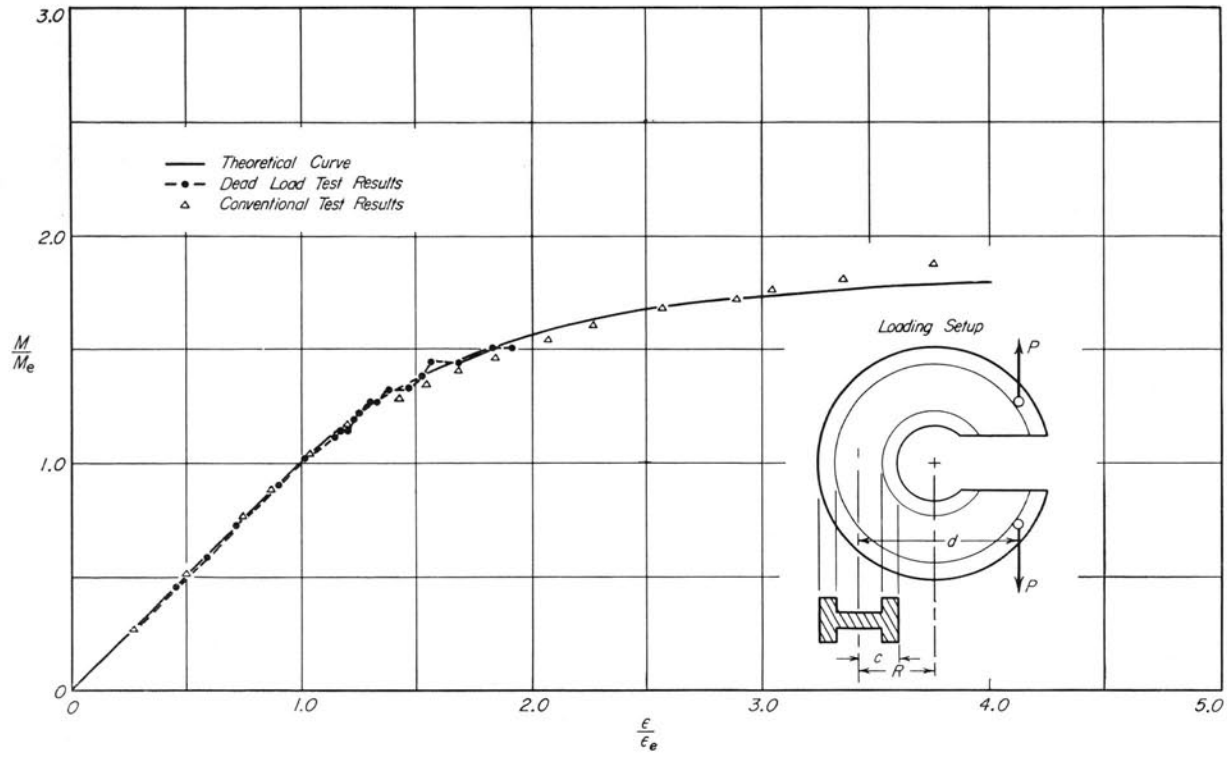


*Fig. 19. Dimensionless Moment-Strain Diagram for Mild Steel Curved Beams 12-S and 13-L Having I-Cross-Sections and R/c Ratios of Approximately 2.00*

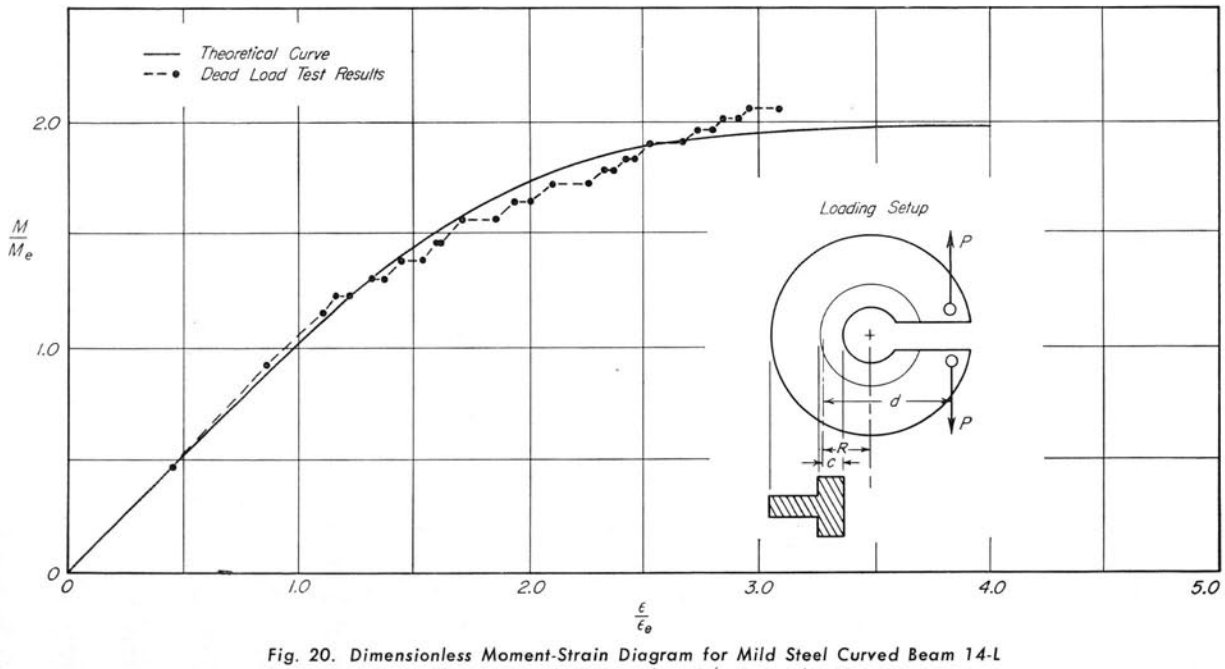


*Fig. 20. Dimensionless Moment-Strain Diagram for Mild Steel Curved Beam 14-L with a T-Cross-Section and an R/c Ratio of 1.60*

intrados only and Eqs. 36 and 37 with $b_1 = b_2$ (see Appendix B) for yielding at intrados and extrados. The curve for the I-beam was obtained by using Eqs. 32 through 43 in Appendix B. The material composing the T-cross-section beam was found to strain-harden in the tension tests; therefore, the theoretical curve was obtained using the same equations as for the I-beam along with Eq. 9.

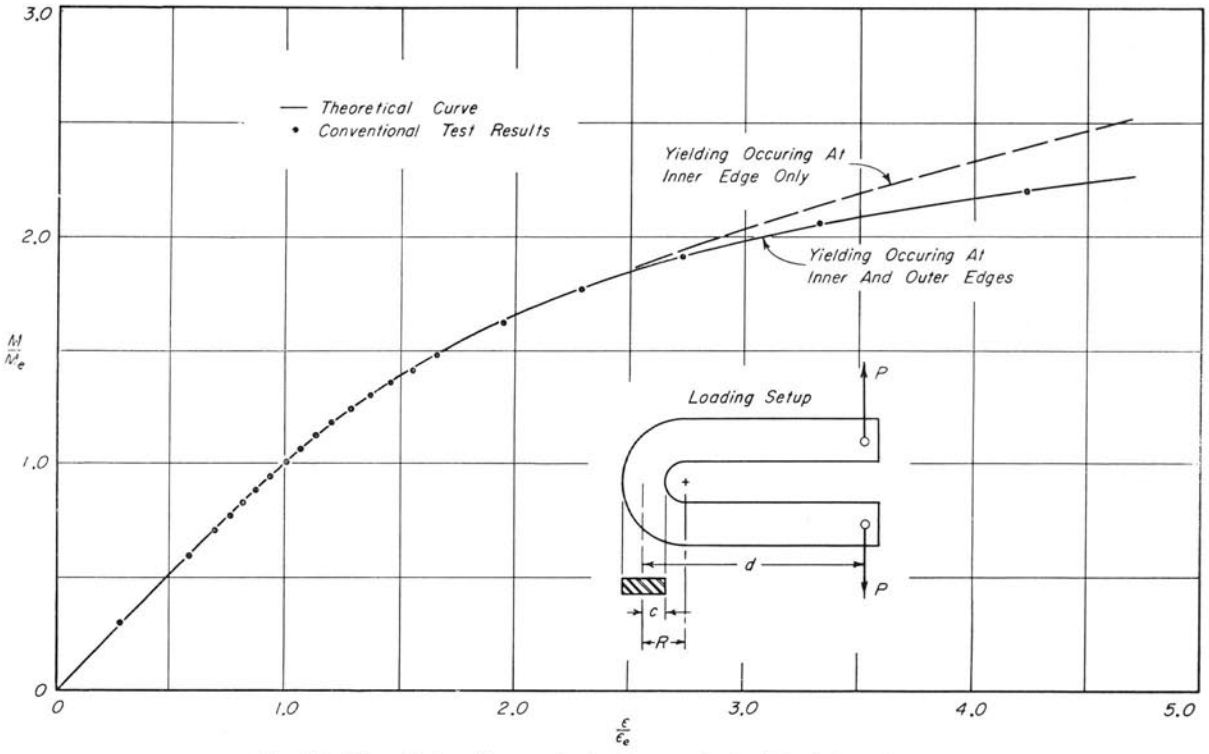


*Fig. 21. Dimensionless Moment-Strain Diagram for Rail Steel Curved Beam 15-S with a Rectangular Cross-Section and an R/c Ratio of 2.11*

Although Eq. 9 is not exact for curved beams, the error involved in using it is small since $\alpha$ was very small for this material.

The theoretical dimensionless moment-deflection curve for the rectangular section beam was obtained by replacing $\epsilon_1/\epsilon_e$ by $\triangle/\triangle_e$, where $\triangle_e$ is the maximum elastic deflection.[16] This relation is only approximate because yielding at the intrados results in a shift of the neutral axis away from the most strained fiber. Even though the computation for $\epsilon_1$ has taken into account the shift of the neutral axis, the above replacement would be valid only if the neutral axis did not shift. For a given $\epsilon$, the computed deflection varies inversely with the distance from the intrados to the neutral axis; hence, the moment-deflection relation errs on the conservative side.

The experimental moment-deformation data for the dead-load tests of the curved beams are shown in the various figures as solid circles joined by dashed lines. Data[17, 18] are also shown for short-time tests of the rectangular and I-cross-section beams by the open triangles in Figs. 18 and 19. Examination of the dead-load test data show the same characteristic stair-step curves as for the straight steel beams. The test data correlate well with the theoretical curves for the rectangular section beam but are somewhat erratic for the tests of the flanged section beams. Because of the complexity of action that takes place in flange-type curve beams, it was not expected that the test data would check the theory; even the elastic solution[12, 13] is somewhat empirical in nature. The strains in the most strained fibers varied in magnitude across the flange. However, using the average of the strain readings taken across the flange for the value of $\epsilon_1$ in the $\epsilon_1/\epsilon_e$ ratio, the data in Figs. 19 and 20 were found to follow the general trend of the theoretical curve.

An annealed rail steel curved beam with rectangular cross section was tested in a screw-powered testing machine (short-time test). The test data for this beam are plotted in Fig. 21. The theoretical curve was plotted by using Eqs. 4, 5, and 9. The results indicate excellent agreement between theory and experiment. Since time effects were found to be less pronounced for curved than for straight beams and since the strain-hardening materials are less time-sensitive, dead-load testing of curved beams of strain-hardening materials was not undertaken.

## V. DISCUSSION OF RESULTS

### 15. Heterogeneous Yielding in Mild Steel Members

As is well known, the inelastic deformation in mild steel members is non-homogeneous.[7, 19, 20, 21, 22, 23] On polished surfaces this non-homogeneity can be seen in the form of yield wedges, usually called Lueder's bands or lines. The material within the boundaries of the Lueder's bands may be strained to a value several times the yield strain, while at the same time the strain in the adjacent surrounding material may have a value lower than the yield strain. To illustrate the foregoing, a short-time test was conducted using a straight beam of rectangular cross-section made from a mild steel material. Strains were measured at various locations over the constant moment section (see Fig. 22) using SR-4 strain gages having ⅛- and ¼-in. gage lengths. In Fig. 22 the Lueder's bands have been painted in order to make them more discernable, and the SR-4 gages have been removed except for that section containing the strain-measuring element. It will be noted that some of the gages were located in regions of elastic material while others had yield wedges under part or most of the strain-measuring element. The number beside each gage gives the strain reading in thousand micro-inches per inch at a post-yield moment of 1.41 $M_e$. Three of the four gages on the top of the beam were still measuring elastic strains at this load. All three gages gave nearly identical readings even though one gage was located on an island of elastic material completely surrounded by yielded material. Since the yield strain, as found from tension specimens cut from the beam following the test, was approximately 900 micro-inches per inch, the strains in these gages indicated that an upper yield point stress was present in the most strained fibers that remained elastic. Since the yield wedges had penetrated to or slightly beyond one-quarter of the depth of the beam at its top and bottom, the strain at this depth might be expected to equal the yield strain; however, the gages on the unyielded regions at this depth indicate somewhat lower strains. The magnitude of the strain indicated by the gages partly covering yield wedges was greater than the yield strain; the larger strains were observed for those gages with the largest percentage of area covered by the yield wedges.

In Figs. 22 and 27, the directions of the Lueder's bands are seen to follow the paths of maximum shearing stress. For a uni-axial state of stress (such as that which occurs in a straight beam subjected to pure bending) there are an infinite number of planes making angles of 45° to the normal stress. Since the beam problem is not a true plane stress problem as assumed in the theory, a small transverse stress of the same sign as the normal stress accompanies the normal stress; therefore, the planes of maximum shearing stress will intersect the neutral surface at an angle of 45 deg. As indicated in Figs. 22 and 27 and as observed in the other beam tests, the Lueder's bands on the tension side of the beam did follow these planes. However, the Lueder's bands on the compression side of the beam were found to follow many other planes making angles of 45 deg to the normal stress.

To further illustrate the heterogeneity of yielding, thirty-two ⅛-in. and eight ¼-in. gage length SR-4 gages were bonded to the mild steel beam of rectangular cross-section which was subjected to the dead-load test. The locations of these gages are shown schematically for one side of the beam in Fig. 23. The strain distribution for the two sides of the beam at each location are shown for each of five test sections. The strains plotted are those which were measured just before applying the load which caused the experimental hinge moment for this beam. It will be noted in Fig. 23 that there are eight ⅛-in. and two ¼-in. gages at each of the four depths investigated which combined give a total gage length of 1.5 in. The average strain at each depth was obtained and plotted at each section as a solid line so that a comparison could be made between these averages and the strains measured with the shorter gage lengths. Three of the four average points are seen to fall on a straight line, whereas the individual gages indicate the non-uniformity of the straining. The basic assumption of the theoretical derivations, i.e., that plane sec-

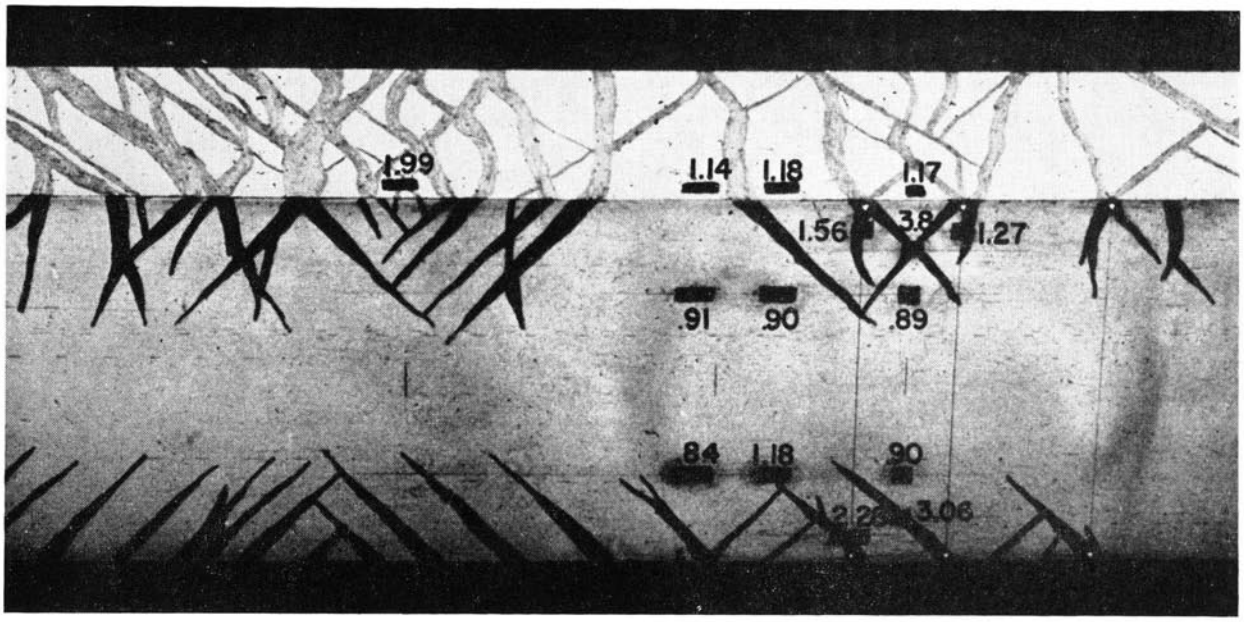


*Fig. 22. Mild Steel Straight Beam with Rectangular Cross-Section Showing Strain Levels in a Field of Heterogeneous Yielding*

tions remain plane, can be considered to be valid only if the deformation is measured over a gage length sufficiently long to give a statistical average of the behavior.

### 16. Peculiarities of Dead-Load Testing

The results presented in Chapter IV for materials which exhibited the heterogeneous yielding (discussed in Section 12) indicate that data from short-time tests corroborate the theoretical analysis outlined in Chapter II, while data obtained from dead-load tests may deviate appreciably from the theory. This deviation manifests itself in the form of two observable peculiarities: (a) an appreciable experimental reduction from the fully plastic load for members made of mild steel, and (b) time effects. The latter included a time delay for the initiation of inelastic deformation upon addition of a load increment after equilibrium was reached at a previous load and a prolonged period of inelastic deformation at a given load. These two topics will be discussed in the following sections.

*a. Experimental Deviation from Fully Plastic Load.* The fully plastic moment for each mild steel

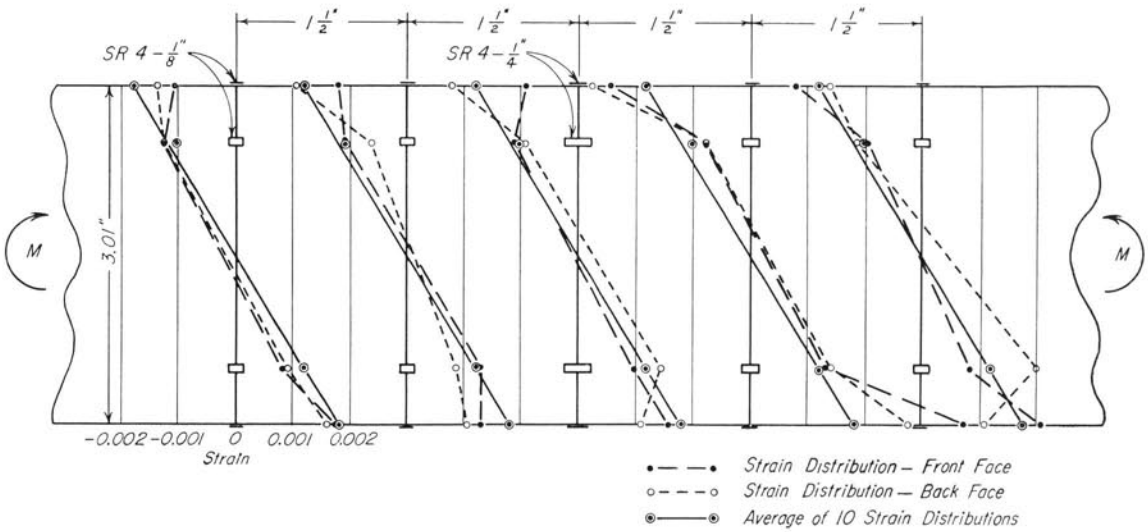


*Fig. 23. Strain Distributions in SAE 1030 Steel Beam After 50 Hours at $M/M_e = 1.28$*

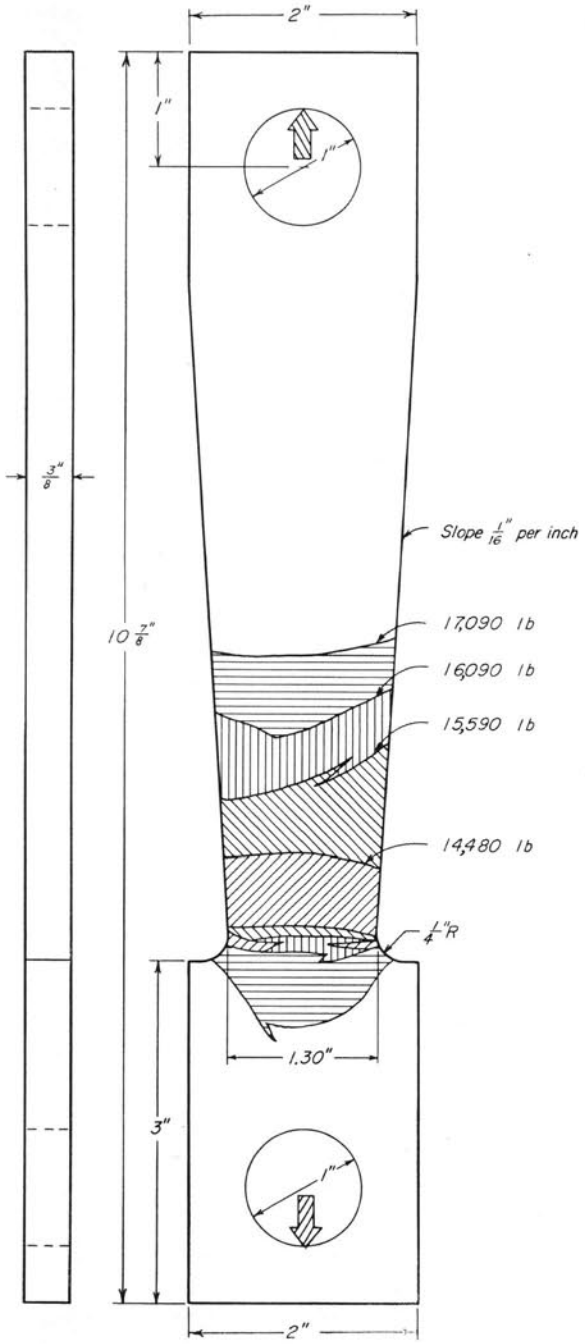


*Fig. 24. Tapered Mild Steel Tension Specimen Showing the Extent of Yielding at Various Dead Loads*

beam was calculated using the lower yield point stress as obtained from standard tension tests. Since the experimental hinge moment for each beam fell below the fully plastic moment, it was reasoned that the lower yield point stress may be reduced by dead-load testing.* To investigate experimentally this line of reasoning, axially-loaded tension members were subjected to dead-load tests in the testing machine shown in Fig. 6. The contour and dimensions of these specimens are shown in Fig. 24. A tension specimen with a constant cross-section was not considered to be feasible for this test because the upper yield point stress must be exceeded before the lower yield point stress can be measured. Once yielding starts in a specimen of constant cross-section, the yielding will spread over the full length of the specimen at the stress that initiated the yielding; this stress might be appreciably above the lower yield point stress for dead-load testing, thus invalidating the purpose of the tests. The tapered specimen was designed so that yielding would be initiated at the minimum cross-section at a stress above the lower yield point stress and then progress into regions of greater cross-sectional area at a lower stress level. Eventually yielding would stop at a section under the lower yield point stress associated with dead-load testing, and this value could then be computed. Furthermore, the same specimen could be used to obtain several values of the lower yield point stress. The angle of taper for the specimen shown in Fig. 24 was such that the maximum stress at any section did not differ from the stresses calculated by the formula $P/a$ by more than 0.2 percent.

Two such tapered specimens were tested in the dead-load machine. The first specimen was subjected to five test loads; the yield stresses at which yielding ceased for these loads were 28,400, 29,000, 28,600, 28,900, and 28,400 lb/in.$^2$ The second specimen was subjected to five test loads resulting in yield stresses of 27,700, 28,400, 28,000, 28,500, and 28,500 lb/in.$^2$ The average of 28,400 lb/in.$^2$ was 9.8 percent below the yield point stresses of 31,500 lb/in.$^2$ as obtained from standard testing of tension specimens taken from the material adjacent to the test specimens. The latter value was obtained from six specimens with variations in yield point stress of less than 2.5 percent.

Although the exact mechanism associated with the reduction in the lower yield point stress by dead-load testing is not known, a qualitative explanation will here be given. As soon as a Lueder's band is formed in an elastic field, the boundaries of the band are limited and controlled by the magnitude of the stress level imposed by the external loads and by the internal resistance in the form of blocking mechanisms which the material may offer to further penetration of the band. These blocking mechanisms, as discussed in Appendix A,

* Some investigations[4, 23, 24] have shown that the magnitude of either the upper or lower yield point stress depends on the speed of testing. Roderick and Phillipps[24] found that the lower yield point stresses for beams and tension specimens were equal if the strain rates in the two types of members were the same.

produce levels of high bond energy between the atoms in the immediate neighborhood of the block. These atoms located in regions of inelastically deformed material may no longer be in definite extended space lattices but show a certain disorder. Since the place change of atoms in such quasi-random orientation is known to be more time-sensitive than in the ordered lattice, place change of atoms will take place if sufficient time is allowed and will result in a reduction of the high bond energy levels associated with the blocking mechanism. With a relief of the high energy bonds, the blocking mechanism is relaxed, allowing a spread of the plastic zone into an elastic region of smaller nominal stress. When the stress level at the front of the plastic zone has been sufficiently reduced, inelastic deformation will not proceed further. The stress level at which inelastic deformation finally ceases is defined as the lower yield point stress by dead-load testing.

For the dead-load straight beam tests of mild steel, the above phenomenon can be used to explain the fact that the experimental hinge moment fell below the fully plastic moment. In mild steel beams the plastic regions appear as yield wedges. As soon as a wedge is formed, the stress distribution through the section at the wedges may be assumed to be similar to distribution $OABC$ in Fig. 25. Stress level $BC$ is the yield point stress as obtained from the standard tension test. As the load is maintained on the beam for a sufficient length of time, the blocking mechanisms along the sides of the wedge are relieved, thus allowing the wedge to broaden. This spreading continues until the stress level throughout the plastic zone reaches the yield point stress associated with dead-load testing. In Fig. 25 this stress level is shown by $B'C$. If the depth of penetration does not increase during this process, the stress at $A$ must increase to some value such as that represented by $A''$ in order to maintain the resisting moment. This would result in a concentration of energy at the tip of the wedge, which would cause a deeper penetration to a depth such as $A'B'$. The resulting stress distribution $OA'B'C$ would provide an internal moment sufficient to balance the external moment. In most instances it was observed that the deepening of the wedge occurred simultaneously with the broadening. At the hinge moment, when the wedges have penetrated close to the neutral axis, the catastrophic yielding results from either a broadening of the wedges, an initiation of new wedges or a combination of the two phenomena. The yield point computed from the experimental hinge moment was found to agree with the yield point determined from the dead-load tests of the tapered tension specimens.

Unlike the straight beams, the test data shown in Figs. 18, 19, and 20 for the curved mild steel beams do not fall below the theoretical curves until large inelastic strains are reached. Due to the fact that curved beams have a steep strain gradient, the strains in the most strained fibers become extremely large before the depth of yielding is sufficient to produce the plastic hinge. For instance, the data shown in Fig. 18 for the curved beam of rectangular cross-section indicates that the strain in the most strained fiber was 4.5 times the elastic strain before the hinge was produced. In comparison, the increase in strain in the straight beam was only 2.2 times the elastic strain before the plastic hinge developed. The comparison between the theoretical fully plastic moment and the experimental hinge moment will be considered only for the curved beam of rectangular cross-section since it is the only curved beam for which sufficient data was obtained. The plastic hinge was found to occur at an $M/M_e$ ratio

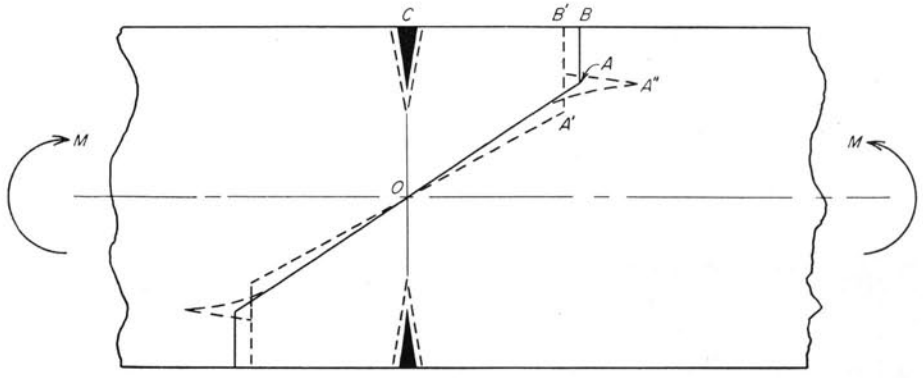


*Fig. 25. Schematic Diagram of a Beam Depicting Growth of Yield Wedges with Time and the Accompanying Changes in Stress Distribution*

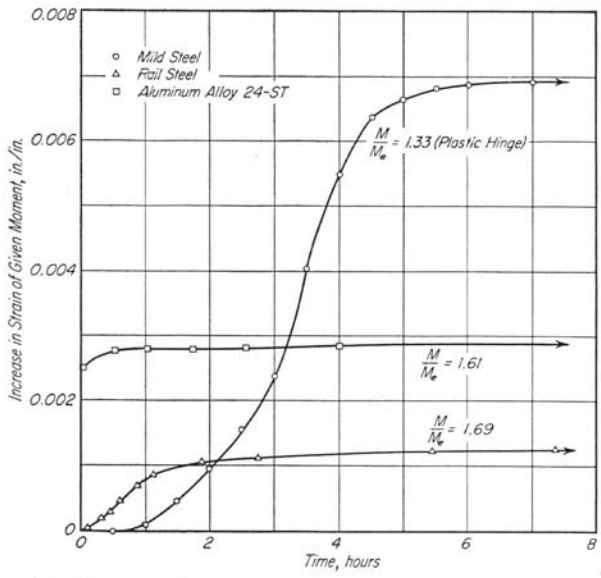


*Fig. 26. Typical Constant Load Time-Deformation Diagrams for Mild Steel, Rail Steel, and Aluminum Alloy 25-ST Straight Rectangular Beams*

of 2.36 as compared to 2.60 for the theoretical fully plastic moment; this is a reduction of 9.2 percent which is about the same reduction as that found for the straight beams and the tapered tension specimens.

*b. Time Effects.* Two other peculiarities of dead-load testing are: (1) the time delay in the initiation of inelastic deformation at a given load, and (2) the duration of inelastic deformation at any given load. A measurable delay was observed only in the tests of the mild steel members. Typical time-deformation diagrams are shown in Fig. 26 for the mild steel, rail steel, and aluminum alloy beams of rectangular cross-section. The curve for the mild steel beam was obtained for the last load increment corresponding to the last stair level shown in Fig. 14. Although the load represented in Fig. 26 by an $M/M_e$ ratio of 1.33 was the load corresponding to the hinge moment, inelastic deformation did not begin at this load until after 30 min had elapsed. Similar time delays were observed for the other two mild steel straight beams, the mild steel curved beams, and the mild steel tension specimens. In the tension specimens, time delays of as much as 5 or 6 hr were observed before inelastic straining started at some of the load increments. The time delay of inelastic deformation in mild steel members depends among other things upon the magnitude of the increase in stress caused by the increment of load. The time delay has been observed for increases in stress of 1000 to 1800 lb/in.$^2$, while other tests indicate that the time delay was eliminated when the increase in stress was 3000 lb/in.$^2$.

The curves shown in Fig. 26 for the rail steel and aluminum alloy beams do not indicate any measurable time delay for initiation of yielding. However the similarity of shape of the curves for the mild steel and rail steel suggests that an extremely short delay might be expected. Inelastic deformation in the rail steel and aluminum alloy beams continued for a long time before ceasing at a given load; the time required for the rail steel was approximately the same as for the mild steel, but the time was much shorter for the aluminum beam to reach a state of equilibrium. The inelastic action in the aluminum alloy was appreciably different from that of the steels. When the load increment was added to the rail steel beam, the deformation proceeded slowly for a while, then speeded up, and finally slowed down again and ceased. For the aluminum alloy beam, when the increment was applied, deformation started at a rapid rate, slowed down, and practically ceased in a period of time which was short in comparison with the steel.

# VI. SUMMARY AND CONCLUSIONS

## 17. Summary

The theoretical load-deformation relations, which have been developed for ductile members subjected to loads which cause inelastic deformation in general, do not include the effect of time on the inelastic behavior. Most of the tests which have been conducted to verify the theory have also neglected time effects.

The purpose of this study was to investigate the time effects associated with dead-load testing of steel and aluminum members. In the inelastic range, each load was maintained until inelastic deformation ceased at that load. The test members included four straight mild steel beams of various cross-sections, three curved mild steel beams of various cross-sections, one straight rail steel (0.8 percent carbon) rectangular beam, and one straight aluminum alloy 24S-T rectangular beam. In most cases test results are also presented for beams subjected to short-time tests, i.e., tests conducted in screw- or hydraulic-powered testing machines. A comparison was made between the test data for the dead-load tests, the test data for the short-time tests, and the theoretical relations.

## 18. Conclusions

1. The moment-strain and moment-deflection diagrams for the beams subjected to dead-load testing were found to be discontinuous rather than smooth curves such as those found for short-time testing. The diagrams for the dead-load testing were found to have a stair-step form.

2. For the straight mild steel beams, the experimental moment-strain and moment-deflection diagrams for dead-load testing were found to lie below the theoretical curves that were based on the conventional tension and compression stress-strain diagrams. This phenomenon is attributed to nonhomogeneous yielding as characterized by Lueder's bands. Similar data for short-time testing of straight mild steel beams were found to check the theory based on homogeneous yielding in the member. The experimental moment-deformation diagrams for the rail steel beam and aluminum alloy 24S-T beams were found to be located on or above the theoretical curves; this was attributed to the fact that rail steel and aluminum yields in a more homogeneous manner and does not exhibit Lueder's bands.

3. Special mild steel tapered tension specimens were also subjected to dead-load testing to determine whether the reduction in strength in the beams was due primarily to the state of stress or to the fact that the lower yield point stress of the material is decreased for members subjected to dead-load testing. The yield stress for the specimens subjected to dead-load testing was 9.8 percent below that obtained from specimens subjected to standard testing techniques.

4. The experimental plastic hinge moments for the three straight mild steel beams fell below the theoretical fully plastic moments by percentages of 12.0, 8.8, and 8.2. Thus the yield point stresses, computed from the beams subjected to dead-load testing, were 12.0, 8.8, and 8.2 percent below the values obtained from standard tension tests.

5. The mild steel curved beam of rectangular cross-section indicated that the yield point was 9.2 percent lower than the value obtained from standard tension tests.

6. From the test results for several types of members made from several mild steels, it may be concluded that the lower yield point stress is reduced about 9 percent when the member is subjected to dead loads.

7. When a load which has produced inelastic deformation is maintained on a mild steel member until inelastic deformation ceases, the material builds up a resistance to immediate inelastic deformation when a small increment of load is added. For increments of load which produced an increase of stress of 1000 to 1800 lb/in.$^2$ in the most strained fibers, inelastic deformation was delayed as much as 30 min in the beam tests. In contrast to the mild steel members, delays for the initiation of inelastic deformation in the rail steel and aluminum alloy beams might have been present but were not

observable by the methods utilized in these experiments.

8. For the steel beams, the major portion of the inelastic deformation at a given load occurred in a period of less than 6 hr. In some cases the inelastic deformation continued for several times this period.

9. The load-deformation behavior of the rail steel was found to be more stable than the mild steel; the aluminum alloy beam was also found to be reasonably stable under dead loads. This may be attributed to the strain-hardening characteristics and the quasi-homogeneous yielding of the material.

# APPENDIX A: QUALITATIVE ANALYSIS OF THE NON-HOMOGENEOUS TIME-SENSITIVE INELASTIC BEHAVIOR OF METALS

The analysis of the inelastic bending of beams presented in this bulletin is based on an idealization of the material behavior. The material is assumed to be isotropic and homogeneous and to obey the stress-strain law illustrated in Fig. 1. The data, photographs (see Fig. 27), and discussion pertaining to time-sensitive behavior and Lueder's bands provide convincing evidence that the material behavior is neither homogeneous nor isotropic; hence, the idealized stress-strain law is only approximate.

A general approach to the problem of inelastic behavior of materials has been suggested by Freudenthal.[25] The inelastic behavior on the macroscopic level of association of matter is made up of the behavior and interaction of the constituent parts on lower levels of association. That is, under a microscope (see Fig. 28) it may be observed that metals are composed of many grains which deform inelastically by a non-homogeneous process known as slip. On the atomic level of association this inelastic deformation is observable only indirectly by X rays. Time- and temperature-sensitive behavior is the result of the transfer of the various forms of energy possessed by atoms on the atomic level of association. This interaction between atoms makes up the behavior of the grains and grain boundaries on the microscopic level.

The discussion that follows is divided into two sections dealing with behavior on the atomic level and behavior on the microscopic level of association of matter. Many investigators studying the various phases of the problem for a number of years have accumulated a vast amount of knowledge; consequently, only those aspects which are directly related to the present problem of non-homogeneous time-sensitive inelastic behavior of metals will be discussed.

### 19. Behavior of Metals on the Atomic Level of Association

*a. Interatomic Forces and Potential Energy.* For the present discussion the atom will be the smallest unit of matter considered. The structure of the atom, that is the nucleus and the surrounding shells of electrons, will not be considered except as their electromagnetic properties create attractive and repulsive forces between atoms. Because of the nature of these forces,[26] atoms of a given material possess an equilibrium spacing where the resultant interatomic force is zero. For spacings closer than the equilibrium spacing, atoms repel one another; similarly for spacings greater than equilibrium, atoms attract one another. When many atoms of a given metal are brought together, they form a crystalline material containing uniformly spaced planes of atoms all held in position by the interatomic forces of the surrounding atoms (see Fig. 29).* The displacement of any atom from its equilibrium position sets up a restorative force which tends to return the atom to its equilibrium position. This equilibrium position represents a position of lowest potential energy; any displacement from this position places an atom in a higher potential energy state.

*b. Thermal Energy.* In addition to potential energy, the atoms possess thermal energy which manifests itself primarily as vibrations of the atoms in the form of kinetic energy. The atoms oscillate about their equilibrium positions with amplitudes that depend upon the amount of thermal energy possessed by the individual atoms. The sum of the kinetic energies of all atoms determines the heat content of a body. At all temperatures above absolute zero, the atoms possess thermal energy and are in constant motion.

The internal forces of a body which resist deformation due to the application of external loads are the interatomic binding forces. Inelastic deformation occurs whenever groups of atoms change place to neighboring positions of lower potential energy after having been displaced to positions of high potential energy due to an applied stress. The

* In Fig. 29 the atomic structure is represented schematically by a bubble model. The nucleus of the atom is assumed to be located at the center of the bubble, and the elastic surface simulates the interatomic forces.

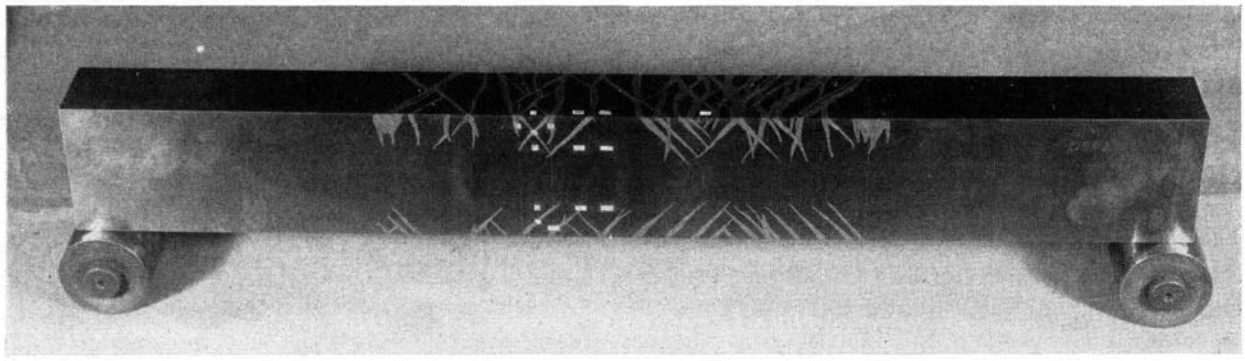

*Fig. 27. Inelastically Deformed Mild Steel Beam Exhibiting Lueder's Bands*

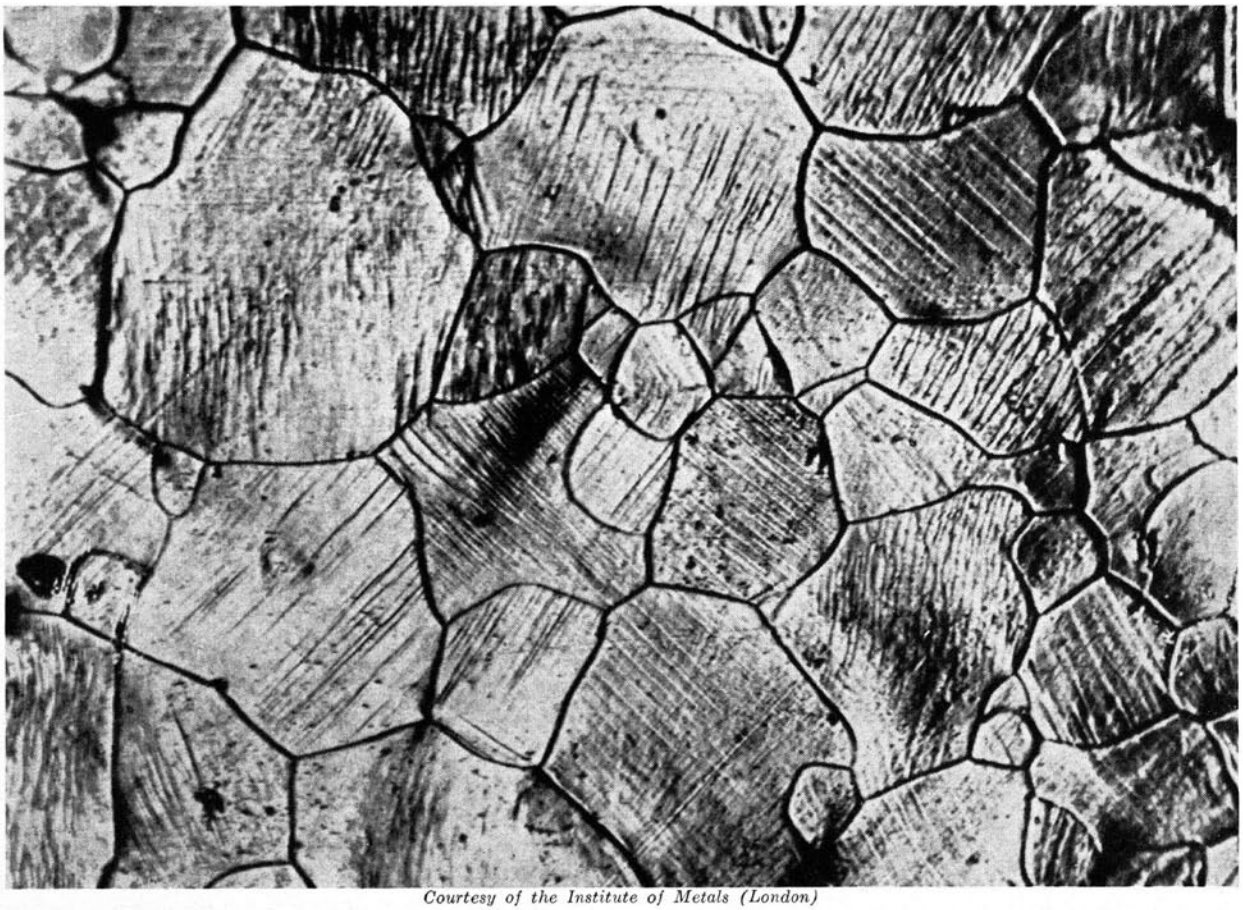

*Courtesy of the Institute of Metals (London)*

*Fig. 28. Inelastically Deformed Iron Exhibiting Slip Bands in the Grains*

role of the thermal oscillations of particles in the process of inelastic deformation becomes clear when it is realized that the energy at which an atom is able to overcome the potential energy barrier and change place to a new position of lower energy is made up of the sum of the strain energy due to external loads and kinetic energy due to thermal oscillations.

To know more specifically what contribution thermal oscillations may make to inelastic deformation, it is necessary to consider the distribution of thermal energy to the atoms. At ordinary temperatures all of the atoms possess thermal energy which is constantly exchanged between the atoms as a result of the atomic interaction forces. At any particular moment a certain number of atoms possess larger amounts of thermal energy than others. Treatment of this problem by the methods of statistical mechanics[27] indicates that, under certain idealizations of the behavior, an exponential

distribution of energy among a group of particles is the most probable or equilibrium distribution. From quantum mechanics[28] it is known that atoms may possess only discrete amounts of energy; consequently, only discrete amounts may be transferred from one atom to another. The exponential distribution of thermal energy to a group of particles is illustrated schematically in Fig. 30. The levels $\epsilon_0$, $\epsilon_1$, $\epsilon_2$, etc. represent the possible energy levels, and the length of the horizontal lines represents the number of atoms possessing this amount of thermal energy. The probability that an atom possesses an amount of thermal energy $\epsilon_r$ is thus given by an equation of the form

$$p = ce^{-\frac{\epsilon_r}{kT}} \qquad (11)$$

where $p$ is the desired probability, $c$ may be considered to be a constant, $k$ is Boltzmann's constant, and $T$ is the absolute temperature. The units of the product $kT$ are energy per particle. It can be seen from Fig. 30 that a small number of atoms possess sufficient energy to make a considerable contribution to the energy required for place change of particles. However, the majority of the atoms are situated in the lower energy levels. At room temperature the thermal energy of the majority of the atoms amounts to only a fraction of the energy required for the place change of particles. At this temperature the influence of thermal oscillations on inelastic deformation is therefore less pronounced unless the applied stress approaches the yield stress of the material.

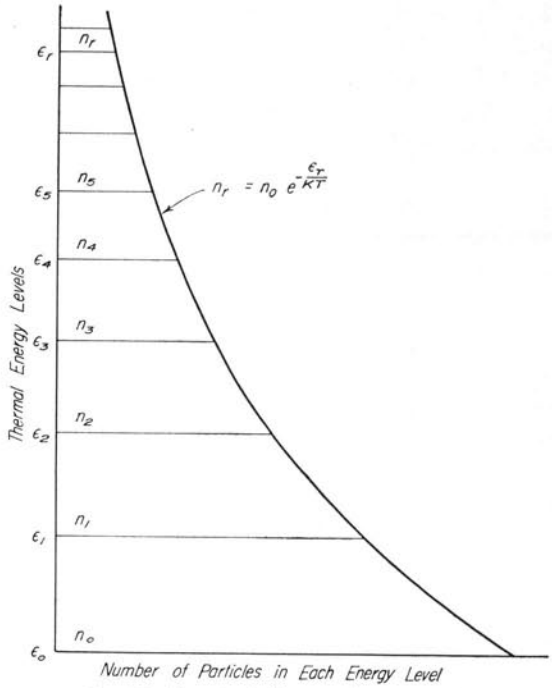


**Fig. 30. Most Probable Distribution of Thermal Energy among a Large Group of Particles**

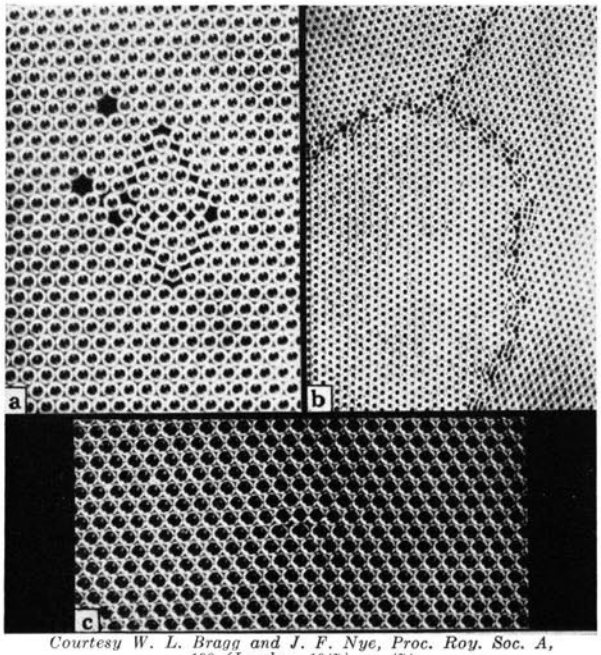


*Courtesy W. L. Bragg and J. F. Nye, Proc. Roy. Soc. A, 190 (London, 1947), p. 474*

**Fig. 29. Bragg's Soap Bubble Model of Atomic Structure Exhibiting (a) Vacancies, (b) Grain Boundaries, and (c) Dislocation**

*c. Inelastic Deformation.* With these ideas as background, it is necessary to consider in more detail the process of slip, that is, a shear displacement that appears to consist of the place change of one whole plane of atoms with respect to the adjoining plane. Theoretical considerations indicate that the external stress required to simultaneously move one plane of atoms with respect to another would require a stress of the order of magnitude of 0.1 of the shear modulus of elasticity.[29, 30] This is from two to three orders of magnitude higher than the observed elastic strength of most pure metals. As previously mentioned, there are too few atoms in sufficiently high thermal energy levels to make up the difference. Thus some other mechanism must account for the observed low yield stress. At present the most successful theories assume various forms of defects in the perfect atomic lattice,[25, 29, 31] as is illustrated in Fig. 29. An extra half plane of atoms is one of the simplest types of defects that will account for the difference between the theoretical and observed elastic strength.[31] This defect, called a dislocation (see Fig. 29c), allows the place change of one row of atoms at a time, thus con-

siderably reducing the external force required to induce slip. The influence of thermal oscillations is still operative on the atoms in the vicinity of the lattice defects, so a temperature dependence is to be expected.[25, 29] The presence of flaws in the crystal lattice has been substantiated by X ray photographs and recently dislocations (screw-type) have been observed in photomicrographs of crystal growth.[31]

Finally, it is necessary to consider the possible influence of alloying elements upon inelastic deformation. For reasons of brevity, this discussion will be limited to a consideration of the interstitial atoms of carbon and nitrogen encountered in all low carbon steels. It has been demonstrated experimentally that the yield point and time delay for initiation of large amounts of inelastic deformation are reduced or eliminated by the removal of the carbon and nitrogen.[32, 33, 34] A widely accepted explanation of this phenomenon is that the smaller carbon and nitrogen atoms diffuse to strategic positions in the lattice and tend to lock or key the slip planes.[35, 36] One theory formulated by Cottrell[37, 38, 39] and based on the dislocation theory suggests that the carbon and nitrogen atoms diffuse to the larger holes on the tension side of a dislocation where they fit somewhat better than in the perfectly ordered lattice. To move the dislocation and produce inelastic deformation requires either (1) a delay time while the carbon or nitrogen atoms diffuse away from the dislocation to a new site of low energy, or (2) a stress sufficiently high to overcome the restraining force on the dislocation due to the presence of the carbon or nitrogen particle. This type of mechanism offers a possible explanation for the upper yield point phenomenon and the avalanche type of inelastic deformation observed with the formation of Lueder's bands. Several of these topics will be discussed further in the next section.

### 20. Behavior of Metals on the Microscopic Level of Association

On the microscopic level the grains and grain boundaries constitute the structural units whose behavior is to be considered. The grains are made up of atoms arranged in a nearly ordered atomic lattice as previously described. However all of the grains contain lattice defects which presumably are responsible for the initiation of inelastic deformation. The grain boundaries are probably not true entities in themselves but form a transition layer from the ordered structure of one grain to an adjoining grain of different orientation.[40] As a transition layer, the grain boundary is made up of atoms arranged in a somewhat unordered pattern. It is the behavior of the individual grains of various orientations modified by their mutual interaction through the grain boundaries that is responsible for the non-homogeneous inelastic time-sensitive behavior observed on the macroscopic level.

*a. Single Crystals.* It is well established that the elastic strength and stiffness of single crystals (large grains) depends upon the relative orientation of the crystal with respect to the applied stress. Briefly, it has been found that slip bands generally occur on atomic planes of greatest density and in a direction parallel to the most dense row of atoms.[41] In metals whose atomic structure is symmetrical, slip may occur on several planes of equal maximum density. In this case the operative slip system is determined by the system sustaining the highest resolved shearing stress.

*b. Grain Boundaries.* Qualitatively the unordered grain boundaries exhibit a quasi-viscous behavior.[42, 43] The atoms making up the grain boundary are in higher, less stable potential energy states than the atoms in the ordered grains. Thus these regions are considerably more sensitive to time and temperature effects than are the grains. A rather successful quantitative treatment of the energy of grain boundaries has been obtained by describing the boundaries as an ordered structure containing a high density of dislocations.[44]

The unordered grain boundaries, viewed as a region containing a high density of dislocations, contain many spaces between atoms on the tension side of the dislocations which are larger than normal. These spaces form ideal positions for alloying or impurity atoms to collect. In steel, for example, many of the carbon and nitrogen atoms presumably collect around dislocations in the grain boundaries as well as those within the grains.[39]

*c. Interaction between Grains.* Inelastic deformation of a polycrystalline aggregate is complicated by the fact that the grains of various orientations are interconnected through the grain boundaries.[40] The formation of a slip band in one grain tends to create a discontinuity or hole when it reaches a grain boundary. A neighboring grain of different orientation cannot slip to conform identically to the changing shape of the first grain, and consequently

the neighboring grain tends to restrain further propagation of the slip band in the first grain.[45, 46, 47] High local stresses are induced in the region of the intersection of the slip band with the grain boundary.[30, 46] These stresses are gradually relaxed by the place change of particles in this region allowing the slip band to progress further. The local disturbance (high stress) created at the grain boundary probably also contributes to the formation of slip bands in the neighboring grains.

In steel, the presence of those carbon and nitrogen atoms around dislocations in the grains and grain boundaries influences the initiation of inelastic deformation. Inelastic deformation commences when the applied stress is sufficiently high to move some of the locked dislocations within the grains (see Section 23). The grain boundaries normally tend to restrain dislocations from moving from one grain into surrounding grains. The presence of carbon and nitrogen appears to increase the restraint offered by grain boundaries. Extensive inelastic deformation apparently is initiated when the restraint of the grain boundaries is overcome or relaxed and slip bands spread or initiate in surrounding grains.[48, 49] This process of spreading inelastic deformation appears to explain qualitatively the origin of Lueder's bands. Once started, this process (yielding) proceeds at a somewhat lower stress, the lower yield point, than the stress required to initiate it, the upper yield point.

The time delay for the initiation of inelastic deformation at stresses below the upper yield point appears to be attributable to the time required for the breakdown of the restraint of the grain boundaries at regions of severe local disturbances.[50, 51, 52,53] When inelastic deformation in the form of Lueder's bands has previously occurred and stopped after a period of time, as in the experiments reported in this bulletin, another time delay is observed when another increment of load is added. The cause of this and subsequent time delays with each load increment may be attributed to aging.[38] The carbon and nitrogen atoms presumably diffuse to the larger-than-normal holes around isolated dislocations, to newly formed slip bands in the grains, and to the grain boundaries. This action stabilizes the regions so that they again tend to restrain the spreading of slip bands from one grain to another.

This discussion is intended as an introduction to some of the ideas upon which a comprehensive theory may be eventually based. The list of references is included to serve as a guide to a more extensive study of this subject.

# APPENDIX B: MOMENT-STRAIN RELATIONS FOR CURVED BEAMS

## 21. Derivation of the Moment-Strain Relation for a Curved Beam of Rectangular Cross-Section

The derivation that follows is based on the assumptions stated in Chapter II, Section 5. The method of approach used is the same as there stated; namely, applying the basic equations of equilibrium to a free body diagram of a section of the loaded beam. For this purpose Fig. 31a shows a curved beam loaded in pure bending and Fig. 31b shows a cut section of the beam with the forces, internal and external, acting as marked. By applying the equations of equilibrium to this cut-section, the following expressions are obtained.

$$\int \sigma \, da = 0^* \tag{12}$$

$$\int (\sigma \, da) \, y = M \tag{13}$$

It can be seen that these expressions contain summations of the resisting forces acting on differential areas over the cut-section and hence cannot be solved until a stress distribution is found that applies for the surface.

The strain distribution for the section is determined by making use of the assumption that plane sections before bending remain plane after bending; the stress distribution follows from the assumption that the fibers in the beam react in a manner similar to those in the conventional tension or compression test in regard to their stress-strain relationships. A study of Fig. 1 will show that these stress-strain relations can be expressed mathematically as follows.

$$\sigma = E\epsilon \tag{14}$$

in the elastic range and

$$\sigma' = (1 - \alpha) \, E\epsilon_e + \alpha E\epsilon \tag{15}$$

in the inelastic range.

To facilitate the development of the relation among the external loading, the stress distribution, and the geometry and dimensions of the beam, part $ABB_1A_1$ of the beam shown in Fig. 31a is enlarged in Fig. 32. Section $AB$ for purpose of analysis is considered as being fixed and therefore all movement due to the bending loads occurs on section $A_1B_1$. The original angle between sections $AB$ and $A_1B_1$ is taken as $d\theta$, and after application of the bending moment section $A_1B_1$ rotates through a small angle $\triangle d\theta$ about the current neutral axis of the beam.

Making use of Fig. 32, it can be seen that the original length of a fiber say $PP_1$ is

$$l = PP_1 = (R_{na} + y) \, d\theta \tag{16}$$

while the total strain in the same fiber is

$$e = P_1P_1' = y \, (\Delta \, d\theta) \tag{17}$$

The unit strain in the fiber is then given by the following expression

$$\epsilon = \frac{e}{l} = \frac{y \, (\Delta \, d\theta)}{(R_{na} + y) \, d\theta} \tag{18}$$

Denoting the ratio of $\Delta d\theta / d\theta$ by $\omega$ and solving this equation for $y$ gives

$$y = \frac{R_{na}\epsilon}{\omega - \epsilon} \tag{19}$$

Differentiating with respect to $\epsilon$ gives

$$dy = \frac{R_{na}\omega \, d\epsilon}{(\omega - \epsilon)^2} \tag{20}$$

The differential area over which the strain in Eq. 18 occurs then is

$$da = b \, dy = \frac{bR_{na}\omega \, d\epsilon}{(\omega - \epsilon)^2} \tag{21}$$

The unknown quantities in the equilibrium equations have been solved for in terms of the dimensions and geometry of deformation of the beam and the geometry of the idealized stress-strain diagram. Equation 12, used to locate the position of the neutral axis at any arbitrary amount of inelastic strain in the fibers at the intrados, will now be set up assuming that yielding is confined to the in-

* If direct loading is used instead of pure bending, this summation would then be written $\int \sigma \, da = P$

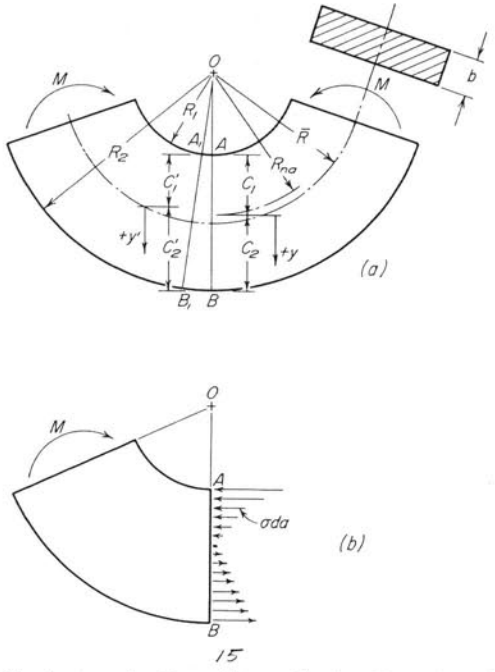


15

*Fig. 31. Rectangular Curved Beam Showing Dimensions, Pure Bending Loading, and Free Body Diagram of a Cut Section*

trados.* Denoting the distance from the neutral axis to the boundary of the inelastic or yielded material as $c_q$, the integral terms are as follows:

$$\int_{c_1}^{c_q} \sigma' b \, dy + \int_{c_q}^{c_2} \sigma b \, dy = 0 \qquad (22)$$

* If yielding starts at the extrados as well, a new derivation is needed to include the presence of the double boundary between elastic and inelastic zones. Equation 36 will simplify to this case.

Equation 13, used to determine the resisting moment over the cross-section at any arbitrary amount of inelastic strain at the intrados, when set up in a similar manner gives

$$\int_{c_1}^{c_q} \sigma' y b \, dy + \int_{c_q}^{c_2} \sigma y b \, dy = M \qquad (23)$$

By substituting Eqs. 14, 15, 19, and 20 into Eqs. 22 and 23, the variables may be reduced to terms of $\epsilon$. By letting $\epsilon_1$ correspond to the strain at the distance $c_1$ from the neutral axis (see Fig. 32), $\epsilon_e$ correspond to the strain at $c_q$, the elastic boundary, and $\epsilon_2$ correspond to $c_2$, the limits of integration are also reduced to terms of $\epsilon$. The equilibrium equations, after these transformations and substitutions are made, become

$$\int_{\epsilon_1}^{\epsilon_e} \left\{(1-\alpha) E\epsilon_e + \alpha E\epsilon\right\} \frac{bR_{na}\omega \, d\epsilon}{(\omega - \epsilon)^2}$$

$$+ \int_{\epsilon_e}^{\epsilon_2} \frac{E\epsilon b R_{na}\omega \, d\epsilon}{(\omega - \epsilon)^2} = 0 \qquad (24)$$

$$\int_{\epsilon_1}^{\epsilon_e} \left\{(1-\alpha) E\epsilon_e + E\epsilon\right\} \frac{bR_{na}^2\omega\epsilon \, d\epsilon}{(\omega - \epsilon)^3}$$

$$+ \int_{\epsilon_e}^{\epsilon_2} \frac{E\epsilon^2 b R_{na}^2\omega \, d\epsilon}{(\omega - \epsilon)^3} = M \qquad (25)$$

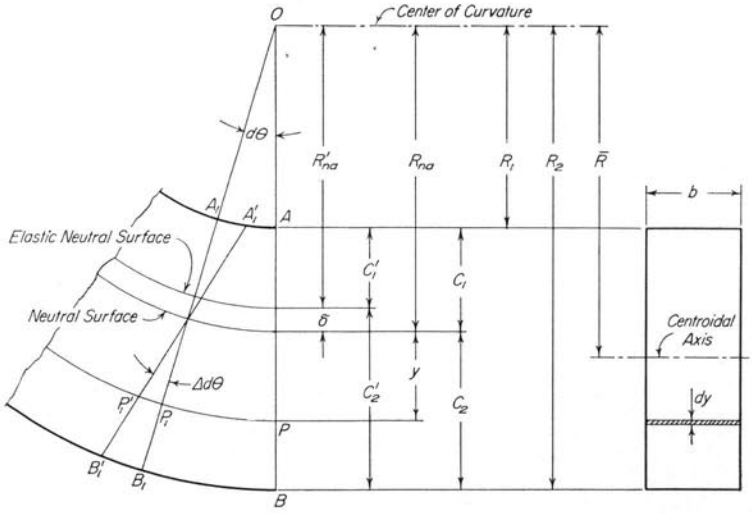


*Fig. 32. Enlarged Cut-Away Portion of Rectangular Curved Beam*

From an observation of Figs. 31 and 32 along with Eq. 18, the following relations can be established:

$$\epsilon_1 = -\omega \frac{c_1}{R_1} \qquad \epsilon_2 = -\frac{R_1}{c_1}\epsilon_1 \frac{c_2}{R_2} \tag{26}$$

If the ratios of $c_1/R_1$ and $c_2/R_2$ are denoted by $n_1$ and $n_2$ respectively

$$\epsilon_1 = -n_1\omega \qquad \epsilon_2 = -\frac{n_2}{n_1}\epsilon_1 \tag{27}$$

Using these equations with the symbol $\lambda$ for the strain ratio of $\epsilon_1/\epsilon_e$, the equilibrium equations, upon integration and simplification, become

$$\frac{(1-\alpha)\,n_1}{\lambda + \lambda n_1} + \alpha\left[\frac{n_1}{1+n_1} + \ln\left(\frac{1+\frac{n_1}{\lambda}}{1+n_1}\right)\right] + \left[\frac{n_2}{1-n_2} + \ln\left(\frac{1-n_2}{1+\frac{n_1}{\lambda}}\right)\right] = 0 \tag{28}$$

$$Eb\omega {R_{na}}^2\left\{(1-\alpha)\left[\frac{-\left(2+\frac{1}{n_1}\right)}{2\lambda\left(1+\frac{1}{n_1}\right)^2} - \frac{1}{\frac{2\lambda}{n_1}+2}\right] - \alpha\left[\frac{3+\frac{1}{n_1}}{2\left(1+\frac{1}{n_1}\right)^2}\right.\right.$$

$$\left.\left. + \ln\left(\frac{1+\frac{n_1}{\lambda}}{1+n_1}\right)\right] + \left[\frac{3{n_2}^2 - 2n_2}{2\,(1-n_2)^2} + \ln\left(\frac{1+\frac{n_1}{\lambda}}{1-n_2}\right)\right]\right\} = M \tag{29}$$

The dimensionless moment-strain relation can be obtained by dividing Eq. 29 by the expression that results when $\lambda$ in Eq. 29 is set equal to unity. The result is as follows:

$$\frac{M}{M_e} = \frac{{R_{na}}^2\lambda {c_1}'}{(\bar{R} - R_{na}')\,c_1\,({c_1}' + {c_2}')}\left\{(1-\alpha)\left[\frac{-\left(2+\frac{1}{n_1}\right)}{2\lambda\left(1+\frac{1}{n_1}\right)^2} - \frac{1}{\frac{2\lambda}{n_1}+2}\right] - \alpha\left[\frac{3+\frac{1}{n_1}}{2\left(1-\frac{1}{n_1}\right)^2}\right.\right.$$

$$\left.\left. + \ln\left(\frac{1+\frac{n_1}{\lambda}}{1+n_1}\right)\right] + \left[\frac{3{n_2}^2 - 2n_2}{2\,(1-n_2)^2} + \ln\left(\frac{1+\frac{n_1}{\lambda}}{1-n_2}\right)\right]\right\} \tag{30}$$

Eqs. 28 and 30 are the two general expressions needed to solve for the moment ratio $M/M_e$ at a particular strain ratio $\epsilon_1/\epsilon_e$ when yielding is confined to the intrados of the rectangular beam. Eq. 30 cannot be evaluated until the neutral axis corresponding to a particular value of the strain ratio is located using Eq. 28. However in Eq. 28 the value of $n_1$ cannot be solved for explicity; therefore a trial and error method suggests itself. Since the neutral axis for the elastic condition is easily computed, two or three judiciously chosen trials will usually yield the correct position of the neutral axis for the inelastic conditions chosen. The solution of these equations as written contain the addition and subtraction of small quantities, and therefore it is necessary to maintain an accuracy of at least four places in all calculations.

It should be realized that the preceding expressions are applicable for beams composed of materials exhibiting strain-hardening characteristics. As stated in Section 8, Eq. 9 gives a simpler method for determining an approximate value of the moment ratio which is sufficiently accurate for most purposes. It is not exact, however, since the neutral axis shifts as yielding progresses through the beam.

### 22. Dimensionless Moment-Strain Relations for Curved Beams Having Cross-Sections Made up of Rectangular Elements

Derivations similar to the one for the rectangular cross-section have been made for cross-sections made up of rectangular elements, for example, the I- and T-cross-sections. The results of these will be listed for the restricted condition of a non-strain-hardening material since the method outlined in Section 9 is available for approximate solutions of other conditions. When changes occur in the width of the cross-section, several different cases must be considered for the progress of yielding through

the member. For instance, in an I-section beam, the following are some of the possibilities for the progress of yielding: (1) yielding confined to the inner flange, (2) yielding occurring within the inner flange and also starting in the outer flange, (3) yielding progressing throughout the inner flange into the web with yielding also starting to occur in the outer flange.

It is apparent then that a group of neutral axis and bending moment equations are necessary to completely cover the inelastic bending of a member made up of rectangular elements. The solutions for six of the most probable cases have been obtained and the results are given. The I-section is used as the example, but imagination will disclose many other cross-sections to which the results apply. In the equations that follow, the definition of most of the terms can be obtained from a reference to Fig. 33. Others involved are defined as follows:

A = cross-sectional area $\quad \lambda = \frac{\epsilon_1}{\epsilon_e} \qquad n_1 = \frac{c_1}{R_1} \qquad n_2 = \frac{c_2}{R_2} \qquad n_3 = \frac{c_3}{R_3} \qquad n_4 = \frac{c_4}{R_4}$ (31)

CASE I. Yielding confined to the inner flange only.

Neutral Axis Equation

$$b_1\left[\frac{1}{\lambda+\frac{\lambda}{n_1}}-\ln\left(1+\frac{n_1}{\lambda}\right)\right]-(b_1-b_2)\left[\frac{n_2}{1+n_2}-\ln(1+n_2)\right]$$

$$+(b_2-b_3)\left[\frac{n_3}{1-n_3}+\ln(1-n_3)\right]+b_3\left[\frac{n_4}{1-n_4}+\ln(1-n_4)\right]=0 \tag{32}$$

Moment-Strain Equation

$$\frac{M}{M_e}=\frac{R_{na}^2\lambda c_1'}{(\bar{R}-R_{na}')\,Ac_1}\left\{b_1\left[\frac{-\left(2+\frac{1}{n_1}\right)}{2\lambda\left(1+\frac{1}{n_1}\right)^2}-\frac{1}{\frac{2\lambda}{n_1}+2}+\ln\left(1+\frac{n_1}{\lambda}\right)\right]\right.$$

$$+(b_1-b_2)\left[\frac{3n_2^2+2n_2}{2(1+n_2)^2}-\ln(1+n_2)\right]+(b_2-b_3)\left[\frac{3n_3^2-2n_3}{2(1-n_3)^2}\right.$$

$$\left.\left.-\ln(1-n_3)\right]+b_3\left[\frac{3n_4^2-2n_4}{2(1-n_4)^2}-\ln(1-n_4)\right]\right\} \tag{33}$$

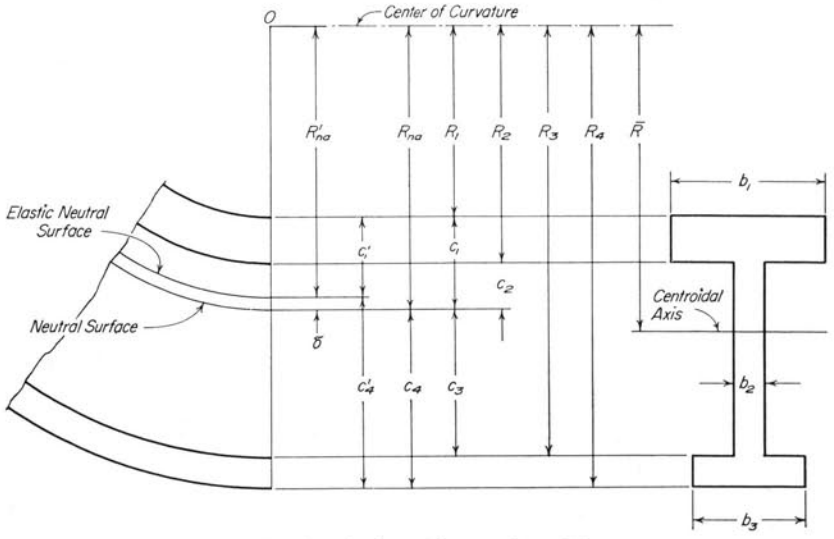


Fig. 33. Sketch of an I-Section Curved Beam

CASE II. Yielding occurring throughout the inner flange and progressing on into the web.

Neutral Axis Equation

$$b_1\left[\frac{1}{\lambda+\frac{\lambda}{n_1}}\right]-(b_1-b_2)\left[\frac{\frac{n_1}{\lambda}}{1+n_2}\right]-b_2\ln\left(1+\frac{n_1}{\lambda}\right)$$

$$+(b_2-b_3)\left[\frac{n_3}{1-n_3}+\ln(1-n_3)\right]+b_3\left[\frac{n_4}{1-n_4}+\ln(1-n_4)\right]=0 \tag{34}$$

Moment-Strain Equation

$$\frac{M}{M_e}=\frac{R_{na}{}^2\lambda c_1'}{(\bar{R}-R_{na}')\,Ac_1}\left\{b_1\left[\frac{-\left(2+\frac{1}{n_1}\right)}{2\lambda\left(1+\frac{1}{n_1}\right)^2}\right]+(b_1-b_2)\left[\frac{2n_2+1}{2\frac{\lambda}{n_1}(1+n_2)^2}\right]\right.$$

$$-b_2\left[\frac{1}{2\frac{\lambda}{n_1}+2}-\ln\left(1+\frac{n_1}{\lambda}\right)\right]+(b_2-b_3)\left[\frac{3n_3{}^2-2n_3}{2(1-n_3)^2}-\ln(1-n_3)\right]$$

$$\left.+b_3\left[\frac{3n_4-2n_4}{2(1-n_4)^2}-\ln(1-n_4)\right]\right\} \tag{35}$$

CASE III. Yielding occurring throughout the inner flange and progressing into the web and also occurring within the outer flange.

Neutral Axis Equation

$$b_1\left[\frac{1}{\lambda+\frac{\lambda}{n_1}}\right]-(b_1-b_2)\left[\frac{\frac{n_1}{\lambda}}{1+n_2}\right]-b_2\ln\left(1+\frac{n_1}{\lambda}\right)$$

$$+(b_2-b_3)\left[\frac{n_3}{1-n_3}+\ln(1-n_3)\right]+b_3\left[\frac{\frac{n_1}{\lambda}}{1-n_4}+\ln\left(1-\frac{n_1}{\lambda}\right)\right]=0 \tag{36}$$

Moment-Strain Equation

$$\frac{M}{M_e}=\frac{R_{na}{}^2\lambda c_1'}{(\bar{R}-R_{na}')\,Ac_1}\left\{b_1\left[\frac{-\left(2+\frac{1}{n_1}\right)}{2\lambda\left(1+\frac{1}{n_1}\right)^2}\right]+(b_1-b_2)\left[\frac{2n_2+1}{2\frac{\lambda}{n_1}(1+n_2)^2}\right]\right.$$

$$-b_2\left[\frac{1}{2\frac{\lambda}{n_1}+2}-\ln\left(1+\frac{n_1}{\lambda}\right)\right]+(b_2-b_3)\left[\frac{3n_3{}^2-2n_3}{2(1-n_3)^2}-\ln(1-n_3)\right]$$

$$\left.+b_3\left[\frac{1}{2-2\frac{\lambda}{n_1}}+\frac{2n_4-1}{2\frac{\lambda}{n_1}(1-n_4)^2}-\ln\left(1-\frac{n_1}{\lambda}\right)\right]\right\} \tag{37}$$

CASE IV. Yielding occurring within the inner flange and also starting in the outer flange.

Neutral Axis Equation

$$b_1\left[\frac{1}{\lambda+\frac{\lambda}{n_1}}-\ln\left(1+\frac{n_1}{\lambda}\right)\right]-(b_1-b_2)\left[\frac{n_2}{1+n_2}-\ln(1+n_2)\right]$$

$$+(b_2-b_3)\left[\frac{n_3}{1-n_3}+\ln(1-n_3)\right]+b_3\left[\frac{\frac{n_1}{\lambda}}{1-n_4}+\ln\left(1-\frac{n_1}{\lambda}\right)\right]=0 \tag{38}$$

Moment-Strain Equation

$$\frac{M}{M_e}=\frac{R_{na}{}^2\lambda c_1'}{(\bar{R}-R_{na}')\,Ac_1}\left\{b_1\left[\frac{-1}{2\frac{\lambda}{n_1}+2}-\frac{2+\frac{1}{n_1}}{2\lambda\left(1+\frac{1}{n_1}\right)^2}+\ln\left(1+\frac{n_1}{\lambda}\right)\right]\right.$$

$$+(b_1-b_2)\left[\frac{3n_2{}^2+2n_2}{2\,(1+n_2)^2}-\ln(1+n_2)\right]+(b_2-b_3)\left[\frac{3n_3{}^2+2n_3}{2\,(1-n_3)^2}\right.$$

$$\left.\left.-\ln(1-n_3)\right]+b_3\left[\frac{1}{2-\frac{2\lambda}{n_1}}-\frac{1-2n_4}{2\frac{\lambda}{n_1}(1-n_4)^2}-\ln\left(1-\frac{n_1}{\lambda}\right)\right]\right\} \tag{39}$$

CASE V. Yielding occurring within the inner flange and also occurring throughout the outer flange and progressing into the web.

Neutral Axis Equation

$$b_1\left[\frac{1}{\lambda+\frac{\lambda}{n_1}}-\ln\left(1+\frac{n_1}{\lambda}\right)\right]-(b_1-b_2)\left[\frac{n_2}{1+n_2}-\ln(1+n_2)\right]$$

$$+b_2\ln\left(1-\frac{n_1}{\lambda}\right)+(b_2-b_3)\left[\frac{\frac{n_1}{\lambda}}{1-n_3}\right]+b_3\left[\frac{\frac{n_1}{\lambda}}{1-n_4}\right]=0 \tag{40}$$

Moment-Strain Equation

$$\frac{M}{M_e}=\frac{R_{na}{}^2\lambda c_1'}{(\bar{R}-R_{na}')\,Ac_1}\left\{b_1\left[\frac{-\left(2+\frac{1}{n_1}\right)}{2\lambda\left(1+\frac{1}{n_1}\right)^2}-\frac{1}{\frac{2\lambda}{n_1}+2}+\ln\left(1+\frac{n_1}{\lambda}\right)\right]\right.$$

$$+(b_1-b_2)\left[\frac{3n_2{}^2+2n_2}{2\,(1+n_2)^2}-\ln(1+n_2)\right]+b_2\left[\frac{1}{2-2\frac{\lambda}{n_1}}-\ln\left(1-\frac{n_1}{\lambda}\right)\right]$$

$$\left.+(b_2-b_3)\left[\frac{2n_3-1}{2\frac{\lambda}{n_1}(1-n_3)^2}\right]+b_3\left[\frac{2n_4-1}{2\frac{\lambda}{n_1}(1-n_4)^2}\right]\right\} \tag{41}$$

CASE VI. Yielding progressing throughout both flanges and starting into the web from both sides.

Neutral Axis Equation

$$b_1\left[\frac{1}{\lambda+\frac{\lambda}{n_1}}\right]-(b_1-b_2)\left[\frac{\frac{n_1}{\lambda}}{1+n_2}\right]+b_2\ln\left(\frac{1-\frac{n_1}{\lambda}}{1+\frac{n_1}{\lambda}}\right)$$

$$-(b_2-b_3)\left[\frac{\frac{n_1}{\lambda}}{1-n_3}\right]+b_3\left[\frac{\frac{n_1}{\lambda}}{1-n_4}\right]=0 \tag{42}$$

Moment-Strain Equation

$$\frac{M}{M_e}=\frac{R_{na}{}^2\lambda c_1'}{(\bar{R}-R_{na}')\,Ac_1}\left\{b_1\left[\frac{-(1+2n_1)}{2\frac{\lambda}{n_1}(1+n_1)^2}\right]+(b_1-b_2)\left[\frac{2n_2+1}{2\frac{\lambda}{n_1}(1+n_2)^2}\right]\right.$$

$$+b_2\left[\frac{-\frac{\lambda}{n_1}}{\left(\frac{\lambda}{n_1}\right)^2-1}-\ln\left(\frac{1-\frac{n_1}{\lambda}}{1+\frac{n_1}{\lambda}}\right)\right]+(b_2-b_3)\left[\frac{2n_3-1}{2\frac{\lambda}{n_1}(1-n_3)^2}\right]$$

$$\left.+b_3\left[\frac{2n_4-1}{2\frac{\lambda}{n_1}(1-n_4)^2}\right]\right\} \tag{43}$$

## APPENDIX C: BIBLIOGRAPHY


1. G. Cook, "The Yield Point and Initial Stages of Plastic Strain in Mild Steel Subjected to Uniform and Non-Uniform Stress Distribution," Phil. Trans. Roy. Soc., Vol. A230, p. 103, 1931.

2. Fujio Nakanishi, "On the Yield Point of Mild Steel," Tokyo Imperial University Aeronautical Research Institute, Report, Vol. 6, p. 81, 1931.

3. G. Bierett, "A Contribution to the Question of Stress Distribution in Bolted Joints," Mitteilungen der deutschen Materialpruefungsanstalten, Sonderheft, XV, 1931.

4. J. L. M. Morrison, "The Yield of Mild Steel with Particular Reference to the Effect of Size of Specimen," Jour. and Proc. Inst. of Mech. Engrs., Vol. 142, No. 3, pp. 192-223, 1943.

5. F. G. E. Peterson, "Effect of Stress Distribution on Yield Points," Proc. Amer. Soc. Civil Engrs., Vol. 72, No. 4, p. 445, 1946.

6. N. Zhudin, "On The Yield Point in Flexure," Zhurnal Tekhnicheskoi Fiziki, Vol. 9, Part 1, p. 968, 1939.

7. Dimitry Morkovin and O. M. Sidebottom, "The Effect of Non-Uniform Distribution of Stress on the Yield Strength of Steel," University of Illinois Engineering Experiment Station, Bulletin Series No. 372, 1947.

8. T. J. Dolan and O. M. Sidebottom, "Raised (?) Yield Point in Bend Tests," Metal Progress, pp. 653-657, Oct. 1947.

9. F. P. Cozzone, "Bending Strength in the Plastic Range," Journal of the Aeronautical Sciences, Vol. 10, No. 5, May 1943.

10. J. Marin and F. D. Cotterman, "Experiments on Plastic Bending for Aluminum Alloy 17S-T," Proc. Amer. Soc. Testing Materials, Vol. 43, 1943.

11. D. O. Brush and O. M. Sidebottom, "Axial Tension and Bending Interaction Curves for Members Loaded Inelastically," Trans. Amer. Soc. Mech. Engrs., Vol. 75, No. 1, pp. 63-72, Jan. 1953.

12. D. C. Broughton, M. E. Clark, H. T. Corten, "Tests and Theory of Elastic Stresses in Curved Beams Having I- and T-Sections," Proc. Soc. of Experimental Stress Analysis, Vol. VIII, No. 1, 1950.

13. C. G. Anderson, "Flexural Stresses in Curved Beams of I- and Box-Sections," Proc. of Institution of Mech. Eng., Vol. 163, 1950.

14. S. Timoshenko, "Strength of Materials, Part II," D. Van Nostrand Co., New York, Chapter 8, pp. 362-395, 1941.

15. W. J. G. Cameron, "An Investigation of the Inelastic Deflection of Beams," unpublished Master's Thesis, University of Illinois, 1948.

16. F. B. Seely and J. O. Smith, "Advanced Mechanics of Materials," John Wiley and Sons, Inc., New York, pp. 167-176, 1952.

17. H. T. Corten, "Tests and Theory of Curved Beams Under Inelastic Strains," unpublished Master's Thesis, University of Illinois, 1947.

18. M. E. Clark, "Tests and Theory of Curved Beams Under Loads that Produce Inelastic Strains," unpublished Master's Thesis, University of Illinois, 1948.

19. H. S. Rawdon, "Strain Markings in Mild Steel Under Tension," Bureau of Standards, Journal of Research, Vol. 1, p. 467, 1929.

20. A. Nadai, "Theory of Flow and Fracture of Solids," McGraw-Hill Book Co., Inc., New York, pp. 49-69, 1950.

21. Julius Miklowitz, "The Initiation and Propagation of the Plastic Zone in a Tension Bar of Mild Steel Under Eccentric Loading," Journ. of Appl. Mech., Vol. 14, No. 1, pp. A21-A29, March 1947.

22. L. H. Donnell, "Plastic Flow as an Unstable Process," J. Appl. Mech., Vol. 9, p. A91, 1942.

23. W. Sylwestrowicz and E. O. Hall, "The Deformation and Aging of Mild Steel," Phys. Soc. Proc., V, Vol. 64, pp. 495-501, 1951.

24. F. W. Roderick and J. H. Phillipps, "Carrying Capacity of Simply Supported Mild Steel Beams," Engineering Structures, Academic Press Inc., New York, pp. 9-48, 1949.

25. A. M. Freudenthal, "The Inelastic Behavior of Engineering Materials and Structures," John Wiley and Sons, Inc., New York, 1950.

26. A. H. Cottrell, "Theoretical Structural Metallurgy," Edward Arnold and Co., 1948.

27. R. W. Gurney, "Introduction to Statistical Mechanics," McGraw-Hill Book Co., Inc., New York, 1949.

28. M. Born, "Atomic Physics," Fourth Edition, English Translation, Blackie and Sons, Ltd., London, 1947.

29. R. Houwink and W. G. Burgers, "Elasticity, Plasticity, and the Structure of Matter," Cambridge University Press, England, 1937.

30. F. R. N. Nabarro, "Influence of Grain Boundaries on the Plastic Properties of Metals," in Recent Developments in Rheology, United Trades Press, Ltd., London, p. 38, 1950.

31. A. H. Cottrell, "Theory of Dislocations," in Progress in Metal Physics, Vol. 1, 1949 and Vol. IV, 1953. Interscience Publishers, New York.

32. J. R. Low and M. Gensamer, "Aging and the Yield Point in Steel," Trans. Amer. Inst. Mining and Metallurgical Engrs., Vol. 158, p. 207, 1944.

33. H. H. Holden and J. Hollomon, "Homogeneous Yielding of Carburized and Nitrided Single Iron Crystals," Trans. Amer. Inst. Mining and Metallurgical Engrs., Vol. 185, p. 179, 1949.

34. C. Wert, "Solid Solubility of Cementite in Alpha Iron," Trans. Amer. Inst. Mining and Metallurgical Engrs., Vol. 188, p. 1242, 1950.

35. M. Gensamer and F. R. Mehl, "Yield Stress of Single Crystals of Iron Under Static Loads," Trans. Amer. Inst. of Mining and Metallurgical Engrs., Vol. 131, pp. 372-377, 1938.

36. C. A. Edwards, D. L. Phillips and Y. H. Liu, "The Yield Point in Steel," Journ. Iron and Steel Inst., Vol. CXLVII, No. 1, p. 145, 1943.

37. A. H. Cottrell, "Effect of Solute Atoms on the Behavior of Dislocations," Report on a Conference on the Strength of Solids, University of Bristol, Physical Society, London, 1948.

38. F. R. N. Nabarro, "Mechanical Effects of Carbon in Iron," Report on a Conference on the Strength of Solids, University of Bristol, Physical Society, London, 1948.

39. A. H. Cottrell, "The Yield Point in Single Crystals and Polycrystalline Metals," in Plastic Deformation of Crystalline Solids, Mellon Institute, Office of Naval Research, 1950.

40. R. King and B. Chalmers, "Crystal Boundaries," in Progress in Metal Physics, Vol. 1, Interscience Publishers, Inc., New York, 1949.

41. E. Schmid and W. Boas, "Plasticity of Crystals," English Translation, F. A. Hughes and Co., London, 1950.

42. Ting-Sui Kê, "Experimental Evidence of the Viscous Behavior of Grain Boundaries in Metals," The Physical Review, Vol. 71, No. 8, p. 533, April 15, 1947.

43. C. Zener, "Elasticity and Anelasticity of Metals," University of Chicago Press, Chicago, Illinois, 1948.

44. W. T. Read and W. Schockly, "Dislocation Models of Crystal Grain Boundaries," in Plastic Deformation of Crystalline Solids, Mellon Institute, Office of Naval Research, 1950.

45. B. Chalmers, "The Influence of the Difference in Orientation of Two Crystals on the Mechanical Effects of Their Grain Boundary," Proc. Roy. Soc., London, A162, p. 120, 1937.

46. W. Boas, "The Interaction Between Crystals of an Aggregate During Plastic Deformation," Proc. 7th International Congress for Applied Mechanics, Vol. 1, 1948.

47. C. A. Edwards, L. B. Pfeil, "The Tensile Properties of Single Iron Crystals and the Influence of Crystal Size on the Tensile Properties of Iron," Journ. Iron and Steel Institute, Vol. 112, p. 79, 1925.

48. W. J. Love, "Structural Changes in Ingot Iron Caused by Plastic and Repeated Stressing," Tech. Report 33 of Research Project "The Behavior of Materials Under Repeated Stress," sponsored by Office of Naval Research, Dept. of Theoretical and Applied Mechanics, University of Illinois, p. 9, 1953.

49. C. S. Roberts, R. C. Carruthers and B. L. Averbach, "The Initiation of Plastic Strain in Plain Carbon Steels," Trans. Amer. Soc. for Metals, Vol. 44, p. 1150, 1952.

50. D. S. Clark and D. S. Wood, "The Time Delay for the Initiation of Plastic Deformation at Rapidly Applied Constant Stress," Proc. Amer. Soc. for Testing Materials, Vol. 49, p. 717, 1949.

51. D. S. Wood and D. S. Clark, "The Influence of Temperature Upon the Time Delay for Yielding in Annealed Mild Steel," Trans. Amer. Soc. for Metals, Vol. 43, p. 571, 1951.

52. D. S. Wood and D. S. Clark, "Delayed Yield in Annealed Steels of Very Low Carbon and Nitrogen Content," Trans. Amer. Soc. for Metals, Vol. 44, p. 726, 1952.

53. T. Vreeland, Jr., D. S. Wood and D. S. Clark, "A Study of the Mechanism of the Delayed Yield Phenomenon," Trans. Amer. Soc. for Metals, Vol. 45, p. 620, 1953.

The Engineering Experiment Station was established by act of the University of Illinois Board of Trustees on December 8, 1903. Its purpose is to conduct engineering investigations that are important to the industrial interests of the state.

The management of the Station is vested in an Executive Staff composed of the Director, the Associate Director, the heads of the departments in the College of Engineering, the professor in charge of Chemical Engineering, and the Director of Engineering Information and Publications. This staff is responsible for establishing the general policies governing the work of the Station. All members of the College of Engineering teaching staff are encouraged to engage in the scientific research of the Station.

To make the results of its investigations available to the public, the Station publishes a series of bulletins. Occasionally it publishes circulars which may contain timely information compiled from various sources not readily accessible to the Station clientele or may contain important information obtained during the investigation of a particular research project but not having a direct bearing on it. A few reprints of articles appearing in the technical press and written by members of the staff are also published.

In ordering copies of these publications reference should be made to the Engineering Experiment Station Bulletin, Circular, or Reprint Series number which is at the upper left hand corner on the cover. Address

THE ENGINEERING EXPERIMENT STATION
UNIVERSITY OF ILLINOIS
URBANA, ILLINOIS